2007

DEVELOPMENT OF ENHANCED CALIBRATION SYSTEM AND MEASUREMENT PROGRAM FOR RADIOSTEREOMETRIC ANALYSIS

Rongyi (Roy) Cai

DEVELOPMENT OF ENHANCED CALIBRATION SYSTEM AND MEASUREMENT PROGRAM FOR RADIOSTEREOMETRIC ANALYSIS

(**Spine Title:** *Enhanced Calibration System and Measurement Program for RSA*)

(**Thesis Format:** Integrated-Article)

By

Rongyi (Roy) Cai

Graduate Program in Medical Biophysics

A thesis submitted in partial fulfillment
of the requirements for the degree of
Master of Science

Faculty of Graduate Studies
The University of Western Ontario
London, Ontario, Canada
September 2007

Abstract

Radiostereometric Analysis (RSA) is the gold standard used to evaluate the performance of Total Joint Replacement. However, the assessment of novel surgical procedures is limited by the present accuracy and precision of RSA. At the same time, complications in the measurement of RSA radiographs confine its large-scale clinical application. The objective of this project is to increase the accuracy and precision of the RSA technique and improve its measurement efficiency. An enhanced calibration cage for RSA was developed by using numerical and image simulations. The phantom study showed that the novel cage has significant improvement of accuracy and precision over two widely used cages. By implementing and modifying existing algorithms, a new measurement program for RSA radiographs was also developed. The program demonstrates equivalent accuracy and precision, and improved user-friendliness, compared to two commercial software applications. The results of this study provide a novel, enhanced RSA technique.

Keywords: Radiostereometric Analysis, accuracy, precision, calibration cage, numerical simulation, computer-synthetic, digital measurement, image processing.

Co-Authorship

The following thesis contains manuscripts prepared for submission for publication within scientific journals. Chapter 2 is an original manuscript that has been submitted for publication in the Journal of Biomechanics, entitled *Development of a RSA calibration system with improved accuracy and precision.* This manuscript is co-authored by Rongyi Cai, Xunhua Yuan, Cecil Rorabeck, Robert B. Bourne, and David W. Holdsworth. Chapter 3 is an original manuscript in preparation for submission, entitled *Development of an automatic measurement program of RSA radiographs*, co-authored by Rongyi Cai, Xunhua Yuan, Cecil Rorabeck, Robert B. Bourne, and David W. Holdsworth.

Rongyi Cai, the Master's candidate, developed and conducted the image simulation procedure, developed the novel measurement program. He also acquired, processed and analyzed data, and wrote the text included in the manuscripts. Dr. Yuan, as co-supervisor and member of the advisory committee, designed the draft version of the new calibration cage, developed and conducted the numerical simulation, helped to acquire, process, analyze data, reviewed the results, provided mentorship, writing and editorial assistance, and guidance for the project. Dr. Holdsworth, as the candidate's co-supervisor, reviewed the manuscripts, provided guidance, mentorship, writing and editorial assistance. Dr. Bourne, as the candidate's supervisor, reviewed the thesis, and provided mentorship. Dr. Rorabeck is the principal investigator of the CIHR/NRC grant that includes the current project and supervises this program. RSA images in this thesis were acquired by Rongyi Cai, Dr. Yuan in the new RSA lab at Robarts Research Institute and the Radiology department, London Health Sciences Centre with the help of Ms. Marg Pavilonis.

Acknowledgements

First of all, I would like to express my heartfelt gratitude to my advisor Dr. Yuan for his guidance on RSA, research, and life in general. This project could not have been completed without his support throughout the entire process. Dr. Holdsworth has also played an important role in this project, his knowledge of radiography, research, and scientific communication skills has proven to be very valuable. And I would like to thank Dr. Boune for his time and support on my master studies.

There have been a number of people whom I would like to express my gratitude to: Aaron So and Bernard Chiu for all the discussions and great times; Louise Du for sharing the experience of this journey; Anne-Marie McColl for the writing and editorial assistance; Damiaan Habets for the discussions of image processing; David McErlain for the thesis template; Patrick Granton for the spectral data of X-ray; Chris Norley for the data backup; Joe Kerr for the assistance of SolidWorks drawings; Marg Pavilonis of Radiology department, LHSC for helping in acquiring RSA images in the research; Chris Vandelaar of machine shop, University of Western Ontario for the new cage fabrication; the entire Holdsworth Lab for the memorable group meetings; and to all my other friends in the lab for making me a part of the great group.

Finally, I am very grateful to my family for their unconditional support. That means a lot to me during the tough time.

Table of Contents

List of Tables

List of Figures

Appendix

List of Abbreviations

2-D.....**Two-Dimensional**

3-D.....**Three-Dimensional**

AFI-RSA.....**Automated Fitting and Identification - RSA**

ANOVA.....**Analysis of Variance**

CP.....**Control Point**

DLT.....**Direct Linear Transformation**

FM.....**Fiducial Mark**

ICDLT.....**Iterative Constrained DLT**

ICDLTI.....**Iterative Constrained DLT and Intersection**

ME.....**Mean Error of Rigid-Body Fitting**

MHF.....**Mexican Hat Filter**

OP.....**Object Point**

PI.....**Prediction Interval**

PMAA.....**Polymethyl Methacrylate**

RSA.....**Radiostereometric Analysis**

SID.....**Source-to-Image Distance**

THA.....**Total Hip Arthroplasty**

THR.....**Total Hip Replacement**

TJR.....**Total Joint Replacement**

1 Introduction

1.1 Background

1.1.1 History of RSA

Radiostereometric Analysis (RSA, Radiostereometry, or Roentgen Stereophotogrammetric Analysis) was introduced by Göran Selvik in 1974, as an accurate method for measuring the three-dimensional (3-D) position of an object using roentgen rays (Selvik, 1974). Since its introduction, the RSA method has been subjected to several amendments to improve its performance (Söderkvist and Wedin, 1993; Nystrom et al., 1994; Ostgaard et al., 1997; Valstar et al., 2000; Börlin et al., 2002). These enhancements helped to transform it from a complex laboratory research technique to an efficient clinical evaluation tool.

By combining the principle of analytic photogrammetry with rigid-body theory, RSA has been proved to be the most accurate, non-invasive radiographic method to determine micromotions between skeleton segments (Kärrholm, 1989; Kärrholm et al., 1997; McCalden et al., 2005). Based on its outstanding capability, RSA has several applications in orthopaedics, pediatrics, odontology and plastic surgery, oncology, rheumatology, anesthesiology, neurosurgery, and hand surgery (Kärrholm, 1989). Most of these studies utilized RSA to assess the micro-movements among bony structures, but it also demonstrated the ability to estimate tumour volume in oncology (Trope et al., 1978). It has been used in animal research to evaluate the performance of hip replacements (Allen et al., 2004).

RSA was originally employed as a research method and clinical tool in Sweden and other Scandinavian countries. It has now become accepted more extensively in North America. World wide, more than 5,000 patients have participated in RSA studies and over 300 scientific papers have been published since the establishment of the RSA technique (Valstar et al., 2005).

1.1.2 Applications of RSA in orthopaedics

The most popular area of RSA practice is orthopaedics; it has been successfully used in orthopaedics for years. RSA studies have been carried out on numerous topics in orthopaedics, including prosthetic fixation, joint stability and joint kinematics, fracture stability, skeletal growth, vertebral motion, and spinal fusion (Kärrholm et al., 1997; Valstar et al., 2005). Even though RSA has been applied to different areas, its practices focus on assessment of Total Joint Replacement (TJR), which includes estimation of implant micromotion, and the measurement of polyethylene wear.

1.1.2.1 Total joint replacement

TJR is the most important and effective treatment for osteoarthrosis. In Canada, the number of TJRs performed in 2004-2005 was 58,714; this represents a ten-year boost of 86.6% from 31,463 in 1994-1995 and a one-year increase of 9.7% from 53,517 in 2003-2004 (Canadian Joint Replacement Registry, 2006). Among all the hip and knee arthroplasty performed in 2004-2005, revision surgery due to the failure of the primary operation accounted for about 9% of all TJRs. Revision surgery not only causes patients a great deal of pain, but it also increases the surgical costs. Patients and the health care system could benefit significantly by improving the performance of TJR.

The main reasons for the failure of TJR treatment are aseptic loosening and polyethylene wear (Canadian Joint Replacement Registry, 2006). To help surgeons select the most appropriate surgical techniques and materials for TJR, and consequently improve its performance, it has been suggested that these techniques and materials should be evaluated before use in large-scale clinical applications (Gross, 1993; Huiskes, 1993).

Unfortunately, regular assessment studies are not suitable in this case, due to the large number of subjects needed and lengthy duration of the studies (Thistlethwaite, 2002). It is inappropriate to treat patients using a technique or material that is still under study. Moreover, the usual follow-up time of 10-15 years (Mäkinen et al., 2004) is too

long for the renovation of the TJR surgical procedure. A quantitative and objective method that can evaluate TJR based on small group studies in a timely manner is necessary. Thanks to its high accuracy, RSA solved the above problems efficiently. We will discuss the successful applications of RSA in the two main fields of TJR assessment, quantifying micromotion of joint implants and measurement of polyethylene wear.

1.1.2.2 Implant micromotion

Implant micromotion measured by RSA usually has two issues, migration, which is the motion that occurs as a function of time, and inducible displacement, which is

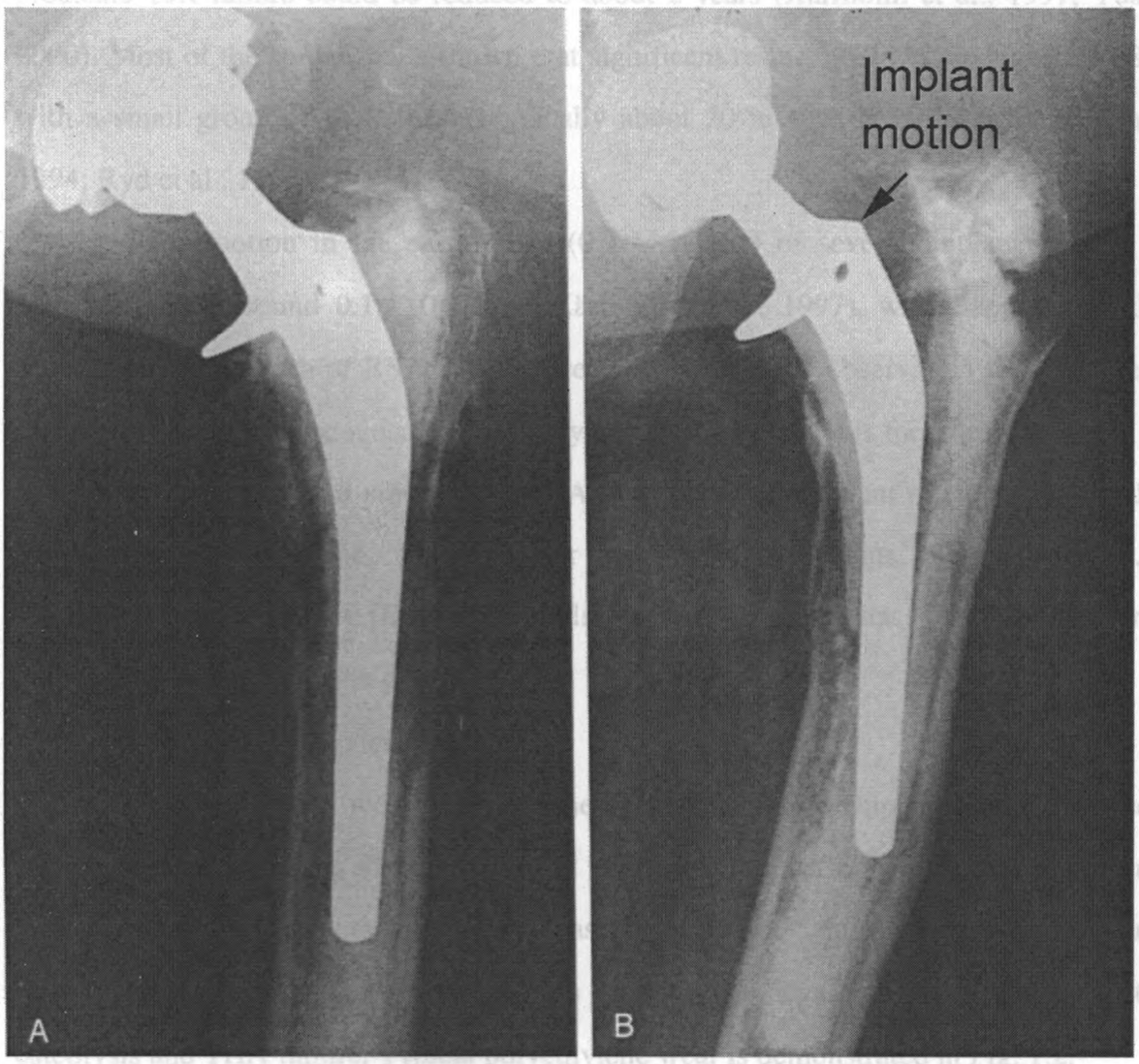

Figure 1.1 A - An early postoperative radiograph of Total Hip Replacement; B - A radiograph taken after 1 year. (In this case, the motion is large for illustrative purpose. Normally, it is much smaller.) Adapted with permission from Freiberg, A. A., 2001. The radiology of orthopaedic implants: an atlas of techniques and assessment. Mosby, St. Louis.

caused by the short-term effects of external forces (Yuan, 2000). Migration exists in hip prosthesis in three forms, movements between the implant and its host bone, subsidence of the femoral stem, and motion of the acetabular cup. In knee prostheses, micromotion is normally just referred to as the micro movements between implant and its host bone. Micromotion in a clinical implant is illustrated (Fig. 1.1).

Two studies have proved the association between implant micromotion, detected by RSA, and long-term aseptic surgery failure (Kärrholm et al., 1994; Ryd et al., 1995). With the current RSA accuracy, the follow-up time to obtain information to reliably predicate TJR failure could be reduced to about 2 years (Kärrholm et al., 1997; Yuan, 2000). Most of the studies have shown that significant results could be obtained by RSA with a small group of participants, typically about 20 in each group (Kärrholm et al., 1994; Ryd et al., 1995).

Micromotion in the early stage (0.5 – 1 year) of several implant designs is observed to be around 0.1 – 0.2 mm (Kärrholm et al., 1997), which approaches the accuracy and precision of RSA. To acquire reliable data, the observation time for these cases may need to be extended to about 2 years after surgery. It is therefore important to improve the accuracy and precision of RSA to measure the implant micromotions in the early stage post-operation, especially for novel implant designs and materials, e.g. VersaBond bone cement (Dalen and Nilsson, 2005), which has very small micro-movements during this time period.

1.1.2.3 Polyethylene wear

Hip polyethylene wear occurs at the bearing surface of hip prostheses, between the femoral head and the acetabular cup. It is one of the most important factors limiting long-term survival of Total Hip Arthroplasty (THA) (McCalden et al., 2005). Debris from polyethylene acetabular components induces the development of periprosthetic osteolysis and THA failure. Typical polyethylene wear is demonstrated in Fig. 1.2.

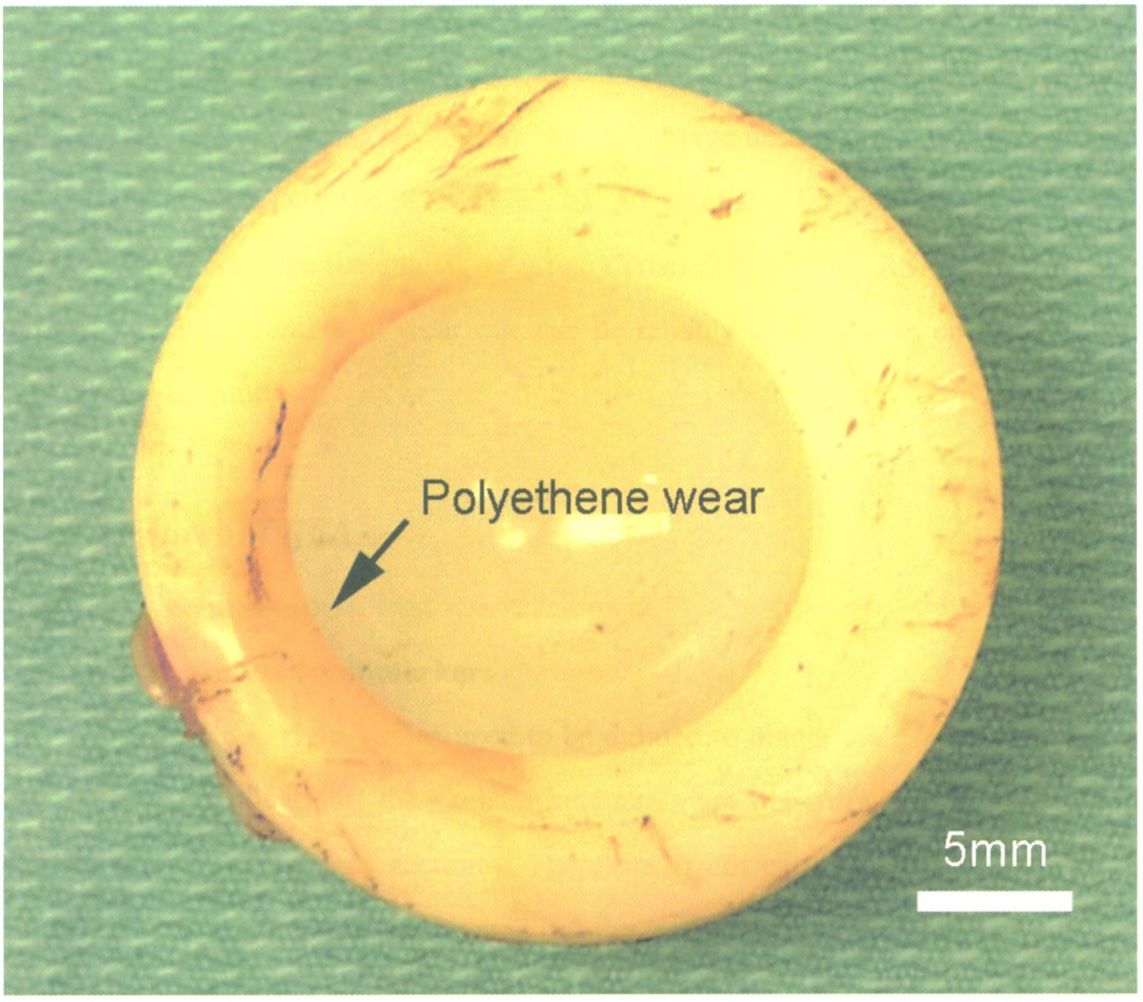

Figure 1.2 An acetabular cup that demonstrates polyethylene wear.

Polyethylene wear could be estimated from the femoral head penetration, relative to the acetabular component. In RSA, wear is measured by computing the relative position between the center of the femoral head and the tantalum markers in the acetabulum (Baldursson et al., 1979). A recent review (McCalden et al., 2005) has concluded that RSA has the best accuracy and precision among the radiographic methods for measuring polyethylene wear after THA. Also, it is best suited for the evaluation of low-wear bearing surfaces at an early follow-up. However, the range of reported annual wear rate of 0.02 – 0.2 mm (Kärrholm et al., 1997) approaches or exceeds the accuracy of RSA. In addition, a threshold wear rate of 0.1 mm per year to observe osteolysis around hip implants was suggested (Dumbleton et al., 2002). The *in vivo* wear rate induced by

bearing surface materials should be below the biologically important threshold for osteolysis. Both the range and threshold of wear rate come close to the accuracy of RSA; this makes the data measured by RSA in the early stage unreliable. It therefore requires years to acquire data, and the investigator has to assume a linear relationship between wear and time to compute the annual wear rate (Yuan, 2000). If the RSA accuracy can be improved, the measurement of wear rate can be reliably conducted in one year or even shorter follow-up time.

1.2 Procedures of RSA

1.2.1 Experiment setup

1.2.1.1 Insertion of markers

To apply RSA, rigid-bodies need to be defined to obtain their real 3-D positions. For orthopaedic applications, the skeletal landmarks are not sufficient to be identified, and provide low measurement accuracy. Therefore, beads called Object Points (OP) are injected into the skeleton and attached to the prosthesis, either during surgery or pre-operatively, to define rigid-body segments. Pin-shaped markers have been used in RSA for facial studies (Rune et al., 1986), but spherical markers are employed in most examinations due to independency of orientation. Typically, the spherical marker is made of tantalum material, which has been proved to possess high biocompatibility (Aronson et al., 1985). Associated with its high atomic number, tantalum is a fairly radio-opaque material and is able to generate significant contrast in RSA radiograph. Markers with diameter of 0.5 mm, 0.8 mm, and 1.0 mm are utilized in RSA applications. There is a tradeoff between marker size and radiographic image quality. Large markers provide more information, but they give a less defined contour and profile, due to the geometric unsharpness caused by finite focal spot size (Valstar et al., 2005). However, markers with diameter of at least 0.8 mm have been suggested in THA due to the fact that the hip is surrounded by thick soft tissues, which reduce the radiograph quality considerably

(Kärrholm et al., 1997). A study has shown that the size (0.8 mm *vs* 1.0 mm) has no influence on the measurement accuracy (Börlin et al., 2002). With respect to the number of markers, at least three non-colinear markers are required to define a rigid body, but 6-9 well scattered markers for each segment are recommended to improve the performance of measurement (Valstar et al., 2005).

In some cases, tantalum markers may not be required in order to apply RSA. For instance, the femoral head of the hip stem, or an indicator inside of the cemented polyethylene acetabular cup can be used to define the implant position in prosthesis studies. Recent developments on a marker-less algorithm (Börlin et al., 2006) and model-based RSA technique (Kaptein et al., 2006) have demonstrated the possibility to utilize RSA without inserting markers. However, their accuracy and precision could not reach as high as regular marker-based RSA.

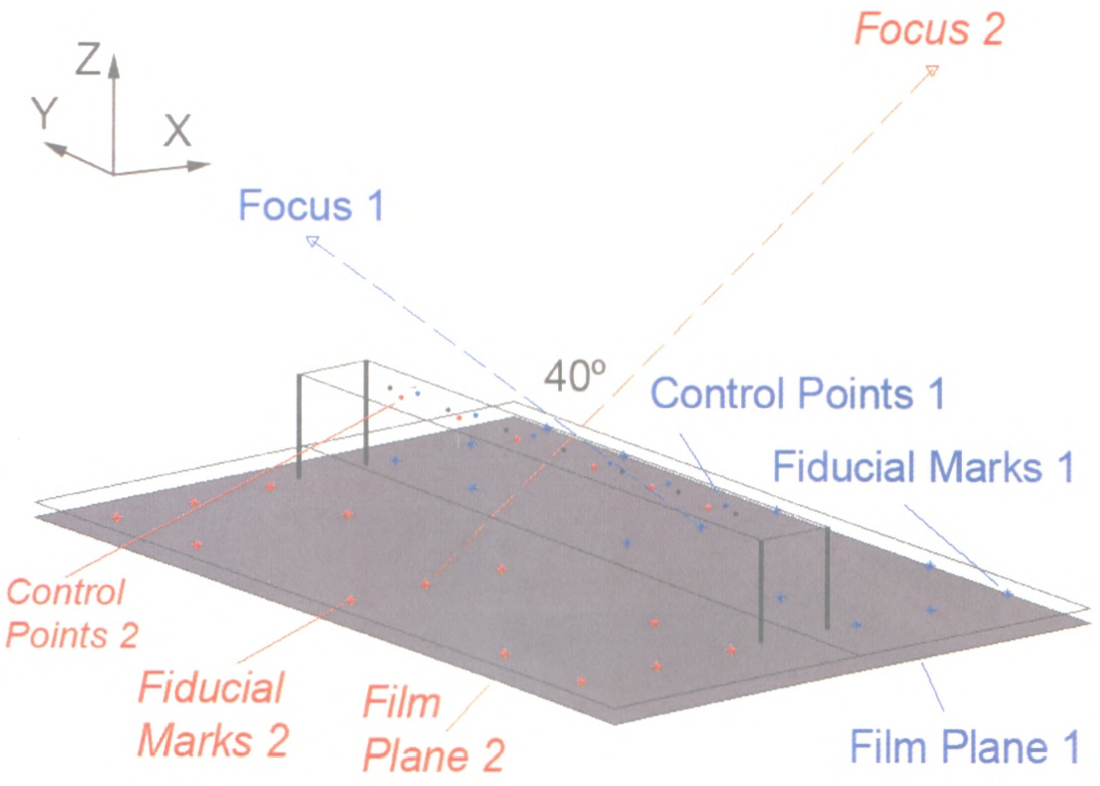

Figure 1.3 Layout of the uniplanar cage.

1.2.1.2 Placement of calibration cage

The calibration cage is the most critical component of the RSA technique. There are two extensively employed commercial cages for RSA, uniplanar and biplanar cages (UmRSA®, RSA Biomedical, Umeå, Sweden). Both types of cages have two identical parts corresponding to the two X-ray views, as required by the stereophotogrammetry principle of RSA. These two parts are placed side-by-side, horizontally with respect to the uniplanar cage and vertically with respect to the biplanar cage, respectively. In each part, two groups of spherical markers, Fiducial Marks (FM) and Control Points (CP) are placed on the cage to allow for calibration. The layout of the uniplanar (Fig. 1.3) and the biplanar cage (Fig. 1.4) are illustrated.

RSA employs two coordinate systems, the two-dimensional (2-D) image coordinate system and the 3-D cage coordinate system. Measurement of RSA radiograph

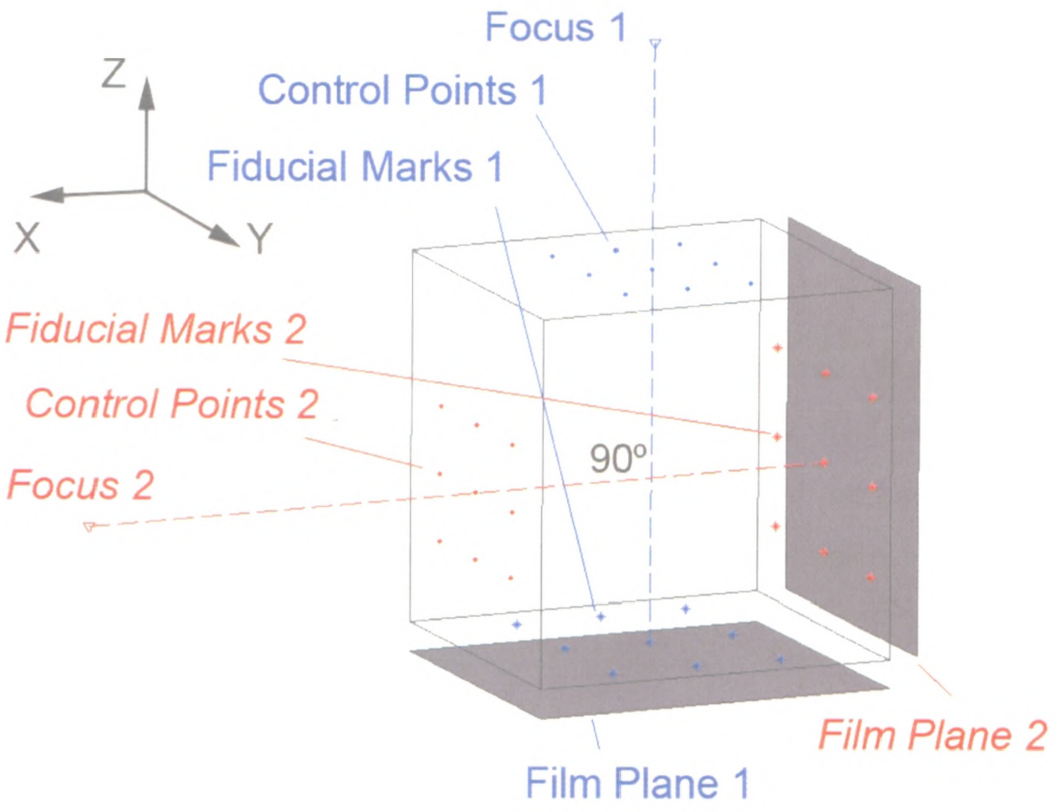

Figure 1.4 Layout of the biplanar cage.

is conducted in the 2-D image coordinate system; the 3-D reconstruction and computation of rigid-body motion are carried out in the cage system, which is defined by calibration markers attached on the cage. To relate these two systems, fiducial marks are used to determine the transformation matrix from image to cage coordinate system. After the FM group is projected onto an X-ray image, the transformation matrix between these two systems can be derived by studying the 2-D image coordinates of fiducial marks on an X-ray image and their predefined 3-D coordinates in the cage system. Another group of control points on the calibration cage is used to determine the position of the X-ray foci. Details of these processes will be discussed in the following sections. Behind each FM plane is a slot to hold either an image cassette or digital detector. The distance between the FM plane and cassette is about 25-35 mm for the uniplanar cage, and 10-20 mm for the biplanar cage, respectively. Potter-Bucky grids are usually attached to the FM plane to reduce the effect of scattered radiation (Yuan, 2000).

The uniplanar calibration cage is mainly used for hip and spine examinations. During measurement, the cage is placed underneath the patient. For examination of the knee, foot, tooth, elbow, or hand, the biplanar cage is employed. The part of the body of interest should be placed inside the biplanar cage.

1.2.1.3 Patient position

It has been suggested that the patient or the body part of interest should be aligned with the cage coordinate system during examination. This must be done during the first measurement or at one of the follow-up evaluations, which will be later used as a reference examination. If at all possible, a standard patient position should be maintained throughout a series of measurements to obtain optimum data (Valstar et al., 2005).

1.2.2 Tuning of X-ray imaging system

To utilize RSA, a conventional X-ray system is adequate. Due to the stereophotogrammetry principle, two sets of X-ray source and detector are required.

Usually, a ceiling-mounted tube and a mobile X-ray machine are employed as the X-ray sources. As for the detector, both film and digital detectors can be used. Digital imaging (computed radiography) has advantages of image display, and storage as well as expediting the process of RSA. It is being used in clinics more extensively (Bragdon et al., 2004). During setup, the angulation of the two X-ray sources should be adjusted to approximately 90 degree for the biplanar setup and 40 degree for the uniplanar setup (Yuan, 2000). These two X-ray beams should intersect at the body structure examined. In clinical application, parameters of the X-ray imaging system have been evaluated and optimized. Typical values used in orthopaedic applications are listed in Table 1.1.

	Hip Measurement	**Knee Measurement**
Focal Spot Size (mm)	0.6 ~ 0.7	0.6 ~ 0.7
X-ray Energy (kVp)	120	90
X-ray Intensity (mAs)	16	2
Focus Film Distance (cm)	140	100

Table 1.1 Typical parameters of RSA radiography in orthopaedic applications at London Health Sciences Centre (University Hospital), London, Ontario, Canada.

1.2.3 X-ray imaging

After set-up, the object will be exposed to X-rays, along with the calibration cage. To reduce any measurement error caused by motion, the stereo exposures are taken simultaneously.

A RSA radiograph is usually taken with a high voltage and low current, compared with a regular diagnostic examination. Therefore, the radiation dose for most RSA exams is much lower than for the corresponding conventional ones (Valstar et al., 2005). The dose of one RSA test for the hip is about 1/10 lower than that of a conventional X-ray examination of the hip (Kärrholm et al., 1997). A typical RSA system setup using uniplanar cage is illustrated in Fig. 1.5.

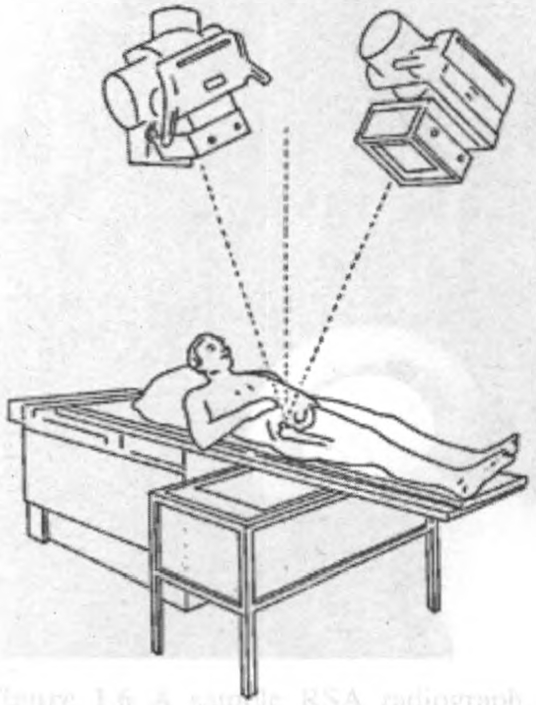

Figure 1.5 RSA examination, using the uniplanar setup. Valstar et al., 2005.

1.2.4 Marker measurement

The only measurement process in RSA is the location detection of calibration and object markers in the radiography image. The exact 2-D location of the marker center in each radiograph should be determined for the future 3-D reconstruction. Since the marker position is the only data acquired from the radiography image, its measurement is one of the most important steps in RSA. Any error in 2-D marker measurement will be propagated, resulting in larger inaccuracies in the subsequent calculations (Yuan, 2000).

There are two ways to measure the marker center, manual and digital. For manual measurement, a highly accurate measuring table is employed. A camera is attached to the table and located over the X-ray film. The camera position can be adjusted so that it is centered on top of a potential marker; the shape of the marker is zoomed by camera and can be matched with a circle on a separate monitor. If they correspond exactly with each other, the position of the camera is then defined as the marker center (Yuan, 2000). Obviously, the process is time consuming and the performance depends on the operator. The theoretic precision of a manual system is 0.01 mm (Selvik, 1989), but it is difficult to achieve that in real examinations.

In the digital system, the image is acquired from a digitized X-ray detector or scanned from radiographic film. A RSA radiograph taken by a digital detector is shown (Fig. 1.6). A computer program is then utilized to measure the marker center at different

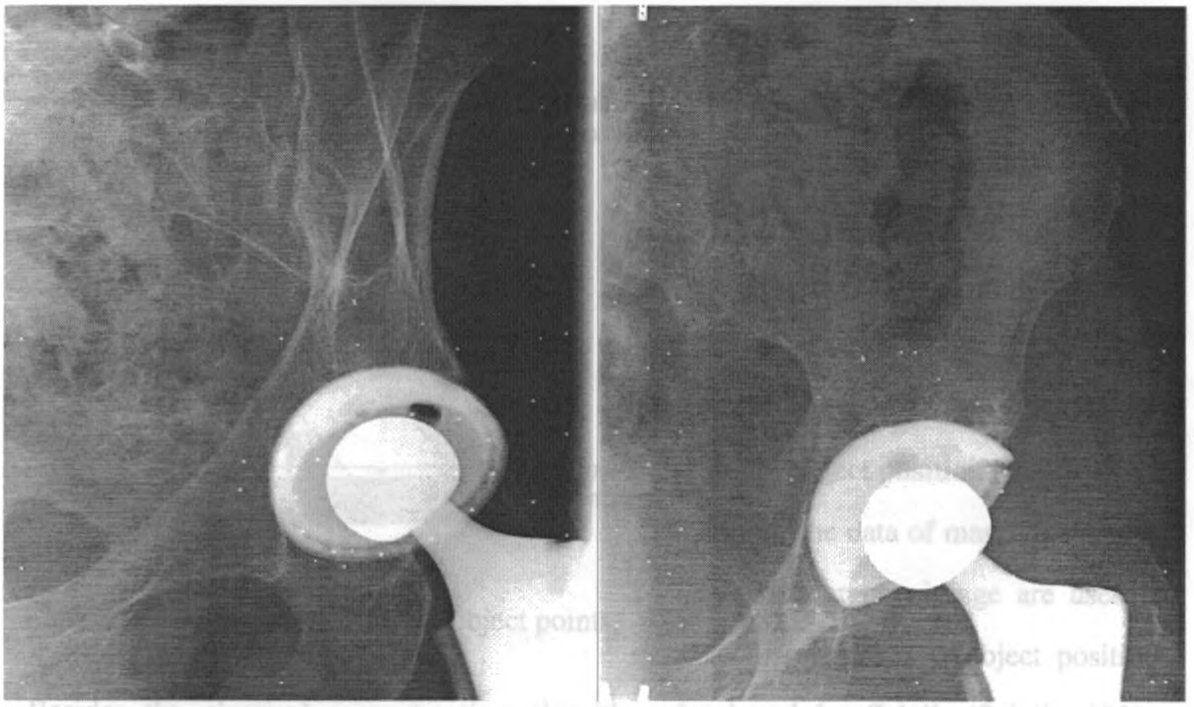

Figure 1.6 A sample RSA radiograph using the uniplanar setup. The left image is generated by X-ray tube on right side, and the right image is generated by left X-ray focus.

automatic levels. The main advantages of digital measurement are a reduction in time and user interactions, and operator independency. It has facilitated the transformation of RSA from a complex research tool to clinical usages. Several research groups have developed digital measurement systems, details of which will be discussed in Chapter 3 of this thesis.

Performance of the digital measurement is comparable with the manual one. A previous study (Börlin et al., 2002) has concluded that digital measurement has improved the precision of RSA for some of the motion parameters. In another examination (Valstar et al., 2000), the digital system produced accuracy comparable with the manual measurement.

Several digital measurement systems have been developed (Ostgaard et al., 1997; Valstar et al., 2000; Olsson, 2001; Börlin et al., 2002; Thistlethwaite, 2002), but their software still shows room to improve, in terms of user-friendliness. In addition, the

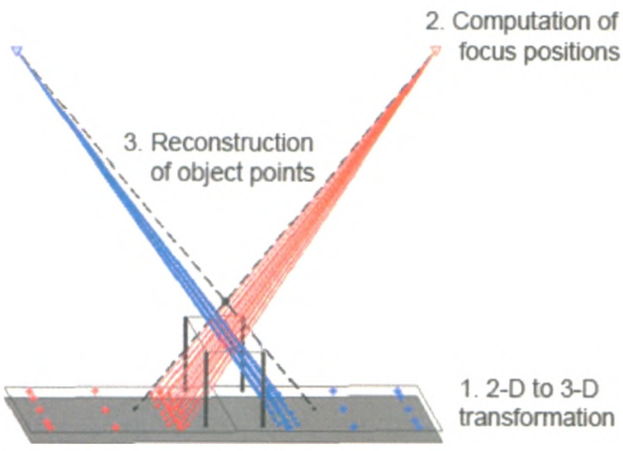

Figure 1.7 3-D reconstruction of object points.

commercial software is limited with respect to their support for new calibration equipment, which means that a RSA image taken with novel cage needs to be measured manually.

1.2.5 Reconstruction of 3-D object positions

The data of marker centers in 2-D radiography image are used to reconstruct the 3-D object position. Besides the classical reconstruction algorithm developed by Selvik (Selvik, 1989), additional new algorithms, including direct linear transformation (DLT) (Choo and Oxland, 2003), Iterative Constrained DLT (ICDLT), and the Iterative Constrained DLT and Intersection (ICDLTI) (Börlin, 2002) have been built up and compared with the traditional version. However, the results are inconclusive (Börlin, 2002) or have not been tested on clinical data (Choo and Oxland, 2003). Due to the advantage of the classical algorithm (Selvik, 1989), which is able to investigate error propagations step by step, we decided to choose it as the reconstruction algorithm in our studies. The algorithm consists of the following processes and is demonstrated in Fig. 1.7.

1.2.5.1 2-D to 3-D transformation

In the first step, by studying the 2-D coordinates of the projected FM in image and their predefined 3-D coordinates on the fiducial plane of the calibration cage, the transformation relationship between the 2-D imaging coordinate system and the 3-D cage coordinate system could be determined. The relationship defines the calibration of coordinates from the imaging system to the cage system.

After defining the calibration, all projected markers, including Fiducial Marks (FM), Control Points (CP), and Object Points (OP) in the radiography image are transferred to the fiducial plane of the cage coordinate system according to the transformation relationship established in the last process.

1.2.5.2 Computation of focus positions

In the next step, the position of the X-ray focal spot is computed. Theoretically, the focus is the intersection of X-rays connecting CP and their projected points on the fiducial plane. However, this does not hold true in real examination due to the finite focal spot size of the X-ray tube and the measurement error of the marker center. The focus is determined as the point which has the least sum of squared distance to lines connecting CP and their corresponding projected points (Selvik, 1989).

1.2.5.3 Reconstruction of 3-D object points

For each object point, there are two projected points on a radiograph, one for each X-ray imaging system, i.e. X-ray focal spot, and detector. By applying the transformation matrix described in the first step, two 3-D coordinates of OP are obtained on the fiducial plane in the cage system. A line connecting the focus and projected OP on the fiducial plane is constructed in each X-ray imaging system. The real 3-D OP coordinates can be found by calculating the intersection point of the two lines (dash lines in Fig. 1.7). Due to measurement error, the 3-D OP is usually considered to be the mid-point of the shortest distance between these two lines. 3-D positioning of implant or bony structure can then be described using 3-D coordinates of inserted OP.

1.2.6 Computation of rigid-body motion

Rigid-body motion can be described as either absolute motion or relative motion. Absolute motion is used to illustrate the movement of a rigid-body at two time points, and relative motion depicts the movement between two rigid-bodies at different times (Yuan, 2000).

In RSA, the relative motion between two rigid-bodies normally refers to the implant and its host bone, or the femoral stem and acetabular cup, as the main objects of study. If we take the radiographic examination at two points in time, the position of each rigid-body at different times can be recorded. The absolute motion of each segment is computed first, and then the relative motion between them can be found. The details have been fully described (Yuan, 2000). Motion can be described in terms of orthogonal translations and rotations, Maximum Total Point Motion, or a rotation about and a translation along the helical axes. It is advisable to present a migration in translations and Euler angular rotations, using 6 degrees of freedom (Valstar et al., 2005). In the RSA computation, all translation components are calculated in combination with the rotation components (Selvik, 1989; Söderkvist and Wedin, 1993), however rotation components are less sensitive to error than translation components (Yuan et al., 1997). Therefore, only the translation components were evaluated in our study.

1.3 Accuracy and precision

1.3.1 Definitions

The terms accuracy and precision in RSA studies were defined in different ways (Biedermann et al., 2001; Önsten et al., 2001; Bragdon et al., 2004). This makes the comparison between methods of measurement difficult. In this thesis, the definition of accuracy and precision was taken from Önsten's study (Önsten et al., 2001). Accuracy was assessed using linear-regression analysis in order to compare the measured values with the true displacements. It was presented as the 95% prediction interval (PI) (Önsten et al., 2001; Madanat et al., 2005; Mäkinen et al., 2005), as obtained by first determining the upper and lower bounds of the prediction interval for each observation, and then calculating the mean of each interval. The details of this procedure are demonstrated in Fig. 1.8. In contrast, precision was calculated as the standard deviation of repeated measurements, under the same conditions.

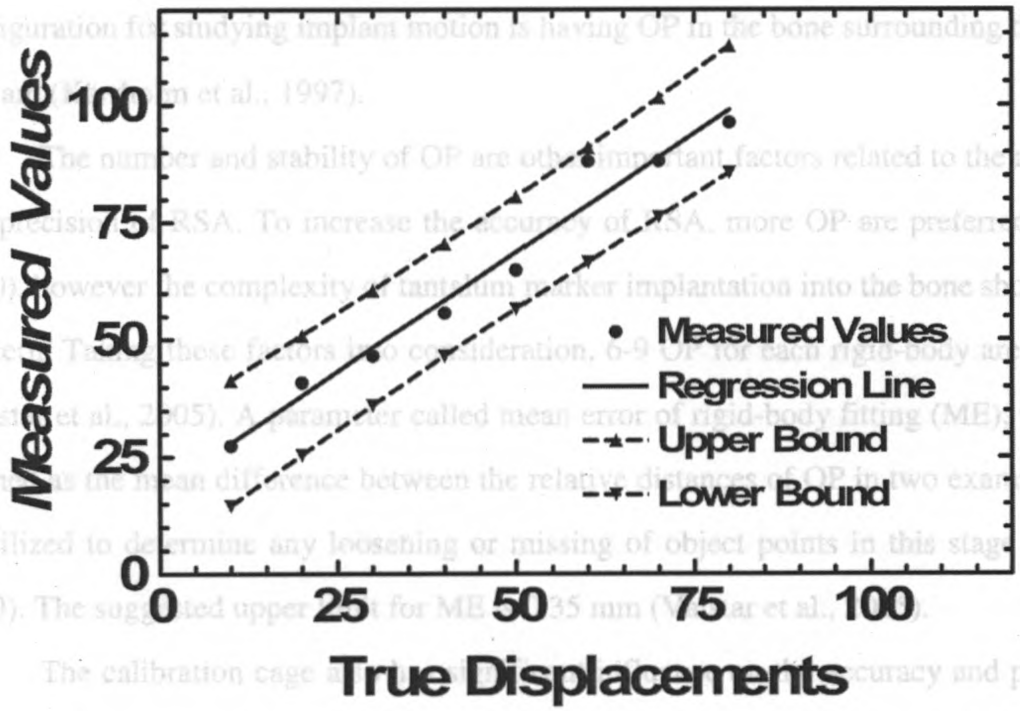

Figure 1.8 Computation of accuracy. The linear-regression analysis was first conducted between the masured values and the true displacements. The upper and lower bounds of the 95% prediction interval was then determined for each observation. The mean of the intervals for each observation was finally reported as the accuracy.

1.3.2 Factors in the setup stage

In the experimental setup stage, the OP positions have an effect on accuracy. By configuring optimal OP positions, the error influence can be minimized (Yuan and Ryd, 2000). Quality of distribution of OP can be evaluated by the condition number (Söderkvist and Wedin, 1993). The use of the condition number in RSA is similar to its use in other contexts of numerical analysis, which is to indicate how numerically well-posed a problem is. A problem is identified as well-conditioned if it has a low condition number, while it is identified as ill-conditioned if it has a high condition number. It was shown that values below 100-110 are very reliable for measurement of prosthetic micromotion (Valstar et al., 2005). An upper limit of 150 for condition number

was recommended. However, a condition number higher than 150 has been used in the examinations of small bones or joints (Ryd et al., 2000). The most favorable configuration for studying implant motion is having OP in the bone surrounding the implant (Kärrholm et al., 1997).

The number and stability of OP are other important factors related to the accuracy and precision of RSA. To increase the accuracy of RSA, more OP are preferred (Yuan, 2000), however the complexity of tantalum marker implantation into the bone should be a concern. Taking these factors into consideration, 6-9 OP for each rigid-body are advised (Valstar et al., 2005). A parameter called mean error of rigid-body fitting (ME), which is defined as the mean difference between the relative distances of OP in two examinations, is utilized to determine any loosening or missing of object points in this stage (Selvik, 1989). The suggested upper limit for ME is 0.35 mm (Valstar et al., 2005).

The calibration cage also has significant influence on the accuracy and precision of RSA. Parameters of the cage design, including bead material (Selvik, 1990) and bead size (Börlin et al., 2002), have been investigated previously. However, other parameters such as the configuration of the calibration setup, bead number, and bead distribution (including bead placement and spacing) have not been fully studied yet.

With respect to precision, it was concluded that it is related to the standardization of radiographic set-up, including positions of X-ray tubes and objects to be measured (Mäkinen et al., 2004).

1.3.3 Factors in the stage of X-ray imaging

The parameters of X-ray exposure, i.e. kVp and mAs, have a large effect on the quality of the RSA radiograph. Eventually, they influence the performance of RSA. These exposure factors have been finalized clinically. In orthopaedic applications of RSA, the objects should be exposed simultaneously to reduce motion effects. Even movements between the bony structure and implant during exposure can be neglected;

the motion of the patient can cause large errors (Selvik, 1990). Angles between X-ray tubes should be considered as well; the ideal angles between two tubes are 90 and 40 for biplanar and uniplanar setups, respectively (Yuan, 2000).

1.3.4 Factors in the stage of marker measurement

Accuracy and precision of the 2-D measurement of radiographic images is one of the most important factors in the RSA system. Measurement error is an original source of inaccuracy and can potentially be propagated in subsequent steps. It increases in the reconstructions of foci and OP, and its effect on the accuracy of the RSA system is notable (Yuan and Ryd, 2000).

The complexity of clinical imaging is a major difficulty in obtaining accurate measurements. The main reason for this problem is the degradation of the radiography image, caused by X-ray scattering, finite focal spot size, and image noise (Bushberg, 2002). Another difficulty is that the projected marker and prosthesis might be very close in the radiograph, making it difficult to distinguish the marker (Börlin et al., 2002).

The ability to find corresponding markers in each image should be taken into account. To apply photogrammetry for the 3-D reconstruction from the 2-D measurement, an OP should have two matching markers on each image (Nystrom et al., 1994). Unmatched markers should be excluded from the study. This is the reason why more than three markers are required in most cases. Occasionally, markers appear to be missing in at least one view, due to overlap with the prosthesis.

1.3.5 Factors in the stage of 3-D OP reconstruction

As described previously, three steps are included in the construction of 3-D OP position. In the first procedure used to determine the 2-D to 3-D transformation, a simulation study has demonstrated that the measurement error is similar before and after the transformation. Therefore, it can be assumed that this step does not affect the

system's performance; error is not propagated during this process (Yuan, 2000). It has also been proven that film deformation will not affect the results of 2-D to 3-D transformation (Selvik, 1989).

1.3.6 Factors in the stage of rigid-body motion

The error in computation of rigid-body motion is related to the distance between segments, and the number of markers in rigid-bodies. When the distance between segments is larger than rigid-body size, translation error has an almost linear relationship with distance (Yuan, 2000). The propagation of rotation error is inversely related to the size of rigid-bodies. As rigid-body size increases, rotation error decreases. Increasing the number of markers on rigid-bodies will decrease the error of both translation and rotation (Yuan, 2000). However, the previously described tradeoff of inserting more markers should be considered.

1.4 Summary

RSA has been proven to be the most accurate *in vivo* 3-D radiographic method for measuring rigid-body micromotions (Kärrholm, 1989; Kärrholm et al., 1997; McCalden et al., 2005). It is most widely accepted in the area of orthopaedics; it has been employed successfully to determine implant micromovements and polyethylene wear for years. Newly developed implant designs, materials, and surgical techniques require improvements to the accuracy and precision of RSA to assess their performance in a timely manner. The accuracy and precision of RSA depends on numerous factors which have been studied extensively, but its relationship with the calibration cage has not yet been fully investigated.

In addition to optimization of RSA cage parameters, it is important to optimize the digital measurement analysis software. Several such software applications have been developed for RSA, but limitations remain. Analysis could be made easier if the

application software became more user-friendly. Furthermore, these software packages do not support novel calibration devices. If a new calibration cage is developed, the RSA radiograph taken with the novel device should be measured manually. This would be a very time-consuming procedure. A fully automated digital RSA measurement program, that is also compatible with newly designed calibration cages, is required.

1.5 Thesis organization

The objective of this study was to improve the function of RSA, including the design of an enhanced calibration system in order to increase the accuracy and precision of RSA and the development of a more user-friendly radiograph measurement program.

Chapter 2 consists of an original article submitted to the *Journal of Biomechanics*. In this manuscript, the relationship between the calibration cage and the performance of RSA are examined thoroughly. The parameters of the calibration system, i.e. configuration of calibration setup, bead number, and bead distribution are investigated using two simulation procedures, numerical simulation and computer-synthetic images, to develop a RSA cage with improved accuracy and precision. Phantom validation of the new cage is also described.

Chapter 3 presents a study of marker measurement in RSA radiography. Algorithms are evaluated, developed, and implemented to build a powerful program. The program is more user-friendly and has equal accuracy and precision, in comparison to commercial software. It is able to support the automated measurement of RSA images taken with the newly designed cage from Chapter 2.

The final chapter concludes the thesis by reviewing the main results, discussing the relevance of Chapters 2 and 3, and investigating the possible direction of future research in relevant fields.

1.6 References

Alfaro-Adrian, J., Gill, H. S., Murray, D. W., 1999. Cement migration after THR. A comparison of charnley elite and exeter femoral stems using RSA. J Bone Joint Surg Br 81(1), 130-4.

Allen, M. J., Hartmann, S. M., Sacks, J. M., Calabrese, J., Brown, P. R., 2004. Technical feasibility and precision of radiostereometric analysis as an outcome measure in canine cemented total hip replacement. Journal of orthopaedic science 9(1), 66-75.

Aronson, A. S., Jonsson, N., Alberius, P., 1985. Tantalum markers in radiography. An assessment of tissue reactions. Skeletal Radiol 14(3), 207-11.

Baldursson, H., Egund, N., Hansson, L. I., Selvik, G., 1979. Instability and wear of total hip prostheses determined with roentgen stereophotogrammetry. Arch Orthop Trauma Surg 95(4), 257-63.

Biedermann, R., Stöckl, B., Krismer, M., Mayrhofer, P., Ornstein, E., Franzen, H., 2001. Evaluation of accuracy and precision of bone markers for the measurement of migration of hip prostheses. A comparison of conventional measurements. J Bone Joint Surg Br 83(5), 767-71.

Börlin, N., 2002. Comparison of resection - intersection algorithms and projection geometries in radiostereometry. ISPRS Journal of Photogrammetry and Remote Sensing 56(5-6), 390-400.

Börlin, N., Rohrl, S. M., Bragdon, C. R., 2006. RSA wear measurements with or without markers in total hip arthroplasty. J Biomech 39(9), 1641-50.

Börlin, N., Thien, T., Kärrholm, J., 2002. The precision of radiostereometric measurements. Manual vs. digital measurements. J Biomech 35(1), 69-79.

Bragdon, C. R., Estok, D. M., Malchau, H., Karrholm, J., Yuan, X., Bourne, R., Veldhoven, J., Harris, W. H., 2004. Comparison of two digital radiostereometric analysis methods in the determination of femoral head penetration in a total hip replacement phantom. J Orthop Res 22(3), 659-64.

Bushberg, J. T., 2002. The essential physics of medical imaging. Lippincott Williams & Wilkins, Philadelphia.

Canadian Joint Replacement Registry, C., 2006. 2006 Report Hip and Knee Replacements in Canada Canadian Institute for Health Information (CIHI).Ottawa, Canada.

Choo, A. M., Oxland, T. R., 2003. Improved RSA accuracy with DLT and balanced calibration marker distributions with an assessment of initial-calibration. J Biomech 36(2), 259-64.

Dalen, T., Nilsson, K. G., 2005. VersaBond bone cement prospective randomized study of the clinical properties of a new bone cement in total knee replacement. Knee 12(4), 311-7.

Dumbleton, J. H., Manley, M. T., Edidin, A. A., 2002. A literature review of the association between wear rate and osteolysis in total hip arthroplasty. J Arthroplasty 17(5), 649-61.

Gross, M., 1993. Innovations in surgery. A proposal for phased clinical trials. J Bone Joint Surg Br 75(3), 351-4.

Huiskes, R., 1993. Failed innovation in total hip replacement. Diagnosis and proposals for a cure. Acta Orthop Scand 64(6), 699-716.

Kaptein, B. L., Valstar, E. R., Spoor, C. W., Stoel, B. C., Rozing, P. M., 2006. Model-based RSA of a femoral hip stem using surface and geometrical shape models. Clin Orthop Relat Res 448, 92-7.

Kärrholm, J., 1989. Roentgen stereophotogrammetry. Review of orthopedic applications. Acta Orthop Scand 60(4), 491-503.

Kärrholm, J., Borssen, B., Lowenhielm, G., Snorrason, F., 1994. Does early micromotion of femoral stem prostheses matter? 4-7-year stereoradiographic follow-up of 84 cemented prostheses. J Bone Joint Surg Br 76(6), 912-7.

Kärrholm, J., Herberts, P., Hultmark, P., Malchau, H., Nivbrant, B., Thanner, J., 1997. Radiostereometry of hip prostheses. Review of methodology and clinical results. Clin Orthop Relat Res(344), 94-110.

Mäkinen, T. J., Koort, J. K., Mattila, K. T., Aro, H. T., 2004. Precision measurements of the RSA method using a phantom model of hip prosthesis. J Biomech 37(4), 487-93.

McCalden, R. W., Naudie, D. D., Yuan, X., Bourne, R. B., 2005. Radiographic methods for the assessment of polyethylene wear after total hip arthroplasty. J Bone Joint Surg Am 87(10), 2323-34.

Nystrom, L., Soderkvist, I., Wedin, P. A., 1994. A note on some identification problems arising in roentgen stereo photogrammetric analysis. J Biomech 27(10), 1291-4.

Olsson, A., 2001. Automatic Roentgen Stereophotogrammetric Analysis. Centre for Mathematical Sciences. Lund University.Lund, Sweden, Master thesis.

Önsten, I., Berzins, A., Shott, S., Sumner, D. R., 2001. Accuracy and precision of radiostereometric analysis in the measurement of THR femoral component translations: human and canine in vitro models. J Orthop Res 19(6), 1162-7.

Ostgaard, S. E., Gottlieb, L., Toksvig-Larsen, S., Lebech, A., Talbot, A., Lund, B., 1997. Roentgen stereophotogrammetric analysis using computer-based image-analysis. J Biomech 30(9), 993-5.

Rune, B., Sarnas, K. V., Selvik, G., Jacobsson, S., 1986. Roentgen stereometry in the study of craniofacial anomalies--the state of the art in Sweden. Br J Orthod 13(3), 151-7.

Ryd, L., Albrektsson, B. E., Carlsson, L., Dansgard, F., Herberts, P., Lindstrand, A., Regner, L., Toksvig-Larsen, S., 1995. Roentgen stereophotogrammetric analysis as a predictor of mechanical loosening of knee prostheses. J Bone Joint Surg Br 77(3), 377-83.

Selvik, G., 1974. A roentgen stereophotogrammetric method for the study of the kinematics of the skeletal system. Lund, Sweden.

Selvik, G., 1989. Roentgen stereophotogrammetry : a method for the study of the kinematics of the skeletal system. Munksgaard, Copenhagen.

Selvik, G., 1989. Roentgen stereophotogrammetry. A method for the study of the kinematics of the skeletal system. Acta Orthop Scand Suppl 232, 1-51.

Selvik, G., 1990. Roentgen stereophotogrammetric analysis. Acta Radiol 31(2), 113-26.

Söderkvist, I., Wedin, P. Å., 1993. Determining the movements of the skeleton using well-configured markers. J Biomech 26(12), 1473-7.

Thistlethwaite, P. A., 2002. Computational methods in RSA: Application to acetabular components of total hip replacements. Mechanical Engineering. University of Calgary, Master thesis.

Trope, C., Selvik, G., Kullander, S., Mattsson, W., Muhlow, A., Astedt, B., 1978. Antineoplastic-drug effect evaluated with a new X-ray stereophotographic measurement of the tumour volume. Ann Chir Gynaecol 67(2), 82-4.

Valstar, E. R., Gill, R., Ryd, L., Flivik, G., Borlin, N., Karrholm, J., 2005. Guidelines for standardization of radiostereometry (RSA) of implants. Acta Orthop 76(4), 563-72. http://www.informaworld.com

Valstar, E. R., Vrooman, H. A., Toksvig-Larsen, S., Ryd, L., Nelissen, R. G., 2000. Digital automated RSA compared to manually operated RSA. J Biomech 33(12), 1593-9.

Vrooman, H. A., Valstar, E. R., Brand, G. J., Admiraal, D. R., Rozing, P. M., Reiber, J. H., 1998. Fast and accurate automated measurements in digitized stereophotogrammetric radiographs. J Biomech 31(5), 491-8.

Yuan, X., 2000. Accuracy analysis of RSA and development of RSPA. Department of Orthopaedics. University of Lund, Ph. D. thesis.

Yuan, X., Ryd, L., 2000. Accuracy analysis for RSA: a computer simulation study on 3D marker reconstruction. J Biomech 33(4), 493-8.

Yuan, X., Ryd, L., Blankevoort, L., 1997. Error propagation for relative motion determined from marker positions. J Biomech 30(9), 989-92.

2 Development of a RSA calibration system with improved accuracy and precision [1]

2.1 Introduction

Radiostereometric analysis (RSA) is the most accurate radiographic method for the analysis of implant motion and wear (Selvik, 1989) and has become the gold standard in orthopaedic clinical studies (Kärrholm, 1989; Kärrholm et al., 1997; McCalden et al., 2005). Recently, many RSA applications have focused on the measurement of small movements (i.e. micromotion) to evaluate newly developed implant design, materials and surgical techniques, such as: cross-linked polyethylene (Digas et al., 2003; Digas et al., 2004), VersaBond bone cement (Dalen and Nilsson, 2005) and different coating materials (Röhrl et al., 2004; Digas, 2005). The clinical and industrial interest in these evaluations, specifically in the early stage of the post-operation (Ryd, 1986; Kärrholm et al., 1994), require an extremely high measurement accuracy and precision. In most cases, these requirements approximate the measurable limitation of the conventional RSA (Ryd et al., 2000), thus bringing uncertainty into the interpretation of the measurement results, and as a consequence, providing motivation for improving the accuracy and precision of the RSA technique itself.

The overall accuracy and precision of RSA technique depends on the performance of each component of the RSA procedure, from synthetic landmark insertion, stereo radiographic examination, radiographic measurement, to the final data analysis (Selvik, 1989; Yuan et al., 1997; Yuan and Ryd, 2000). Many studies have been performed to improve the outcome of these RSA steps. For the procedure of synthetic landmark

[1] A version of this chapter has been submitted for publication (Cai, R., Yuan, X., Rorabeck, C., Bourne, R., and Holdsworth, D.W., 2007. Development of a RSA calibration system with improved accuracy and precision. J Biomech.

insertion, Selvik (Selvik, 1989) outlined the advantages of using spherical beads due to the orientation independence, and tantalum material due to its optimal radiographic performance and biocompatibility with human tissue. For the radiographic measurements, previous manual systems have been upgraded to digital format (Vrooman et al., 1998; Börlin et al., 2002). Previous studies on digital systems have confirmed that bead size and image resolution have no influence on the measurement accuracy, after comparing two sizes of beads (0.8 mm *vs* 1.0 mm) (Börlin et al., 2002) and different image resolutions (Valstar et al., 2000). With respect to data analysis, Selvik and Yuan (Selvik, 1989; Yuan and Ryd, 2000) revealed the pattern of error propagation in three-dimensional (3-D) reconstruction, while Woltring and Yuan (Woltring et al., 1985; Yuan et al., 1997) detailed the influence of segment size and number of marker beads. Söderkvist (Söderkvist and Wedin, 1993) introduced the concept of condition number into the RSA calculation to assess bead placement.

While previous studies have optimized specific steps in the RSA process, few investigations have focused on the importance of the RSA calibration cage in the stereo radiographic examination. RSA examination uses two patient radiographs, acquired simultaneously by two X-ray units and requires a calibration cage used during image acquisition to provide highly accurate position localization. Although the calibration cage is identified as a crucial factor determining the performance of stereo examination, the quantitative relationship between cage design and the accuracy and precision of RSA is unclear. Our clinical RSA experience suggests that currently available RSA calibration cages are not optimal.

We believe that the RSA technique is capable of higher accuracy than previous reports, which is about 100 μm (Kärrholm, 1989; Ryd et al., 2000). By optimizing the parameters of the calibration system, RSA accuracy and precision can be improved. In order to test our hypothesis, we conducted this study by developing a new RSA calibration cage system. Computer simulation techniques were applied to design the new

cage and to predict its performance in advance. The computer simulation techniques were used because they were capable of identifying individual factors that may influence RSA accuracy and precision, and also allowed us to evaluate design concepts before final fabrication (Yuan et al., 1997; Yuan and Ryd, 2000; Choo and Oxland, 2003). In the end, an *in vitro* experimental validation was conducted to assess the performance of our new cage, by comparing the accuracy and precision of the new calibration cage with two widely used clinical cages. A highly accurate knee-joint phantom was used in the experimental comparison, in order to assess the cage performance in a realistic way.

2.2 Methods

The main parameter of an RSA calibration system is the configuration of the calibration setup (i.e. relative geometry of the calibration cage, patient and X-ray sources). Clinically, two RSA configurations are available; one is a uniplanar setup for large joints, such as the hip and spine (Kärrholm, 1989; Kärrholm et al., 1997), and the other is a biplanar setup, for small joints, such as the knee, elbow and ankle (Kärrholm, 1989; Selvik, 1989). Each configuration has different calibration cage systems, designed for different research purposes; however, whether these cage systems provide the same accuracy and precision is unclear. In fact, no comparison has been performed so far to explore the similarity and difference among these cages. In addition to the calibration setup, the following key parameters are related to the cage design: bead size, bead material, bead distribution (i.e. bead placement and spacing), and bead number. Bead size and material have been studied previously (Selvik, 1990; Börlin et al., 2002), but the bead distribution and bead number have not been fully investigated yet.

Therefore, in our study, we focused on the parameters of calibration configuration, bead distribution, and bead number. In practice, these parameters are constrained by several factors. The configuration and bead distribution are limited by the size of radiographs and the source-to- patient distance. Bead number is constrained by the

complexity of physical fabrication and expense. To achieve an optimal design under these constraints before the physical construction, a numerical simulation and computer-synthetic image techniques were developed and implemented.

2.2.1 Numerical simulation

Numerical simulation for RSA has been previously described in detail (Yuan et al., 1997; Yuan and Ryd, 2000; Choo and Oxland, 2003; Garling et al., 2005). In brief, clinical RSA measurement data are simulated as true two-dimensional (2-D) image coordinates, which are then perturbed by random errors in both u- and v- directions. The true coordinates are obtained by perspectively projecting all cage markers and object points from a 3-D space to a fiducial plane. The random errors in image coordinates are assumed as normal distributions along both u- and v- axes, calculated once, and then stored in an error matrix for repeated use in numerical simulation.

2.2.2 Parameter optimization

Numerical simulation was employed to optimize the parameters. The type of configuration is the first parameter we investigated. In order to design the new cage optimally and match clinical constraints, we first analyzed the calibration cages that are currently in use with two commercial RSA packages (UmRSA Digital Measure® v2.2.1, RSA Biomedical, Umeå, Sweden and RSA-CMS® v4.0, Medis, Leiden, The Netherlands). For each cage design studied, the location of control points and fiducial marks was determined from the cage configuration files provided by the RSA analysis software packages. The analysis was performed under the same conditions, i.e., the same error matrix, the same segments placing at the optimal position of cage systems (i.e. intersection of two X-ray beams) and zero motion between two segments (Yuan et al., 1997; Yuan and Ryd, 2000; Choo and Oxland, 2003).

Bead distribution was then investigated. Both the fiducial marks and control points were placed near the edge of the fiducial and control planes, respectively, in a rectangular pattern. The reason to locate the fiducial mark peripherally is that the distance of each marker to the center is proportional to the accuracy of the transformation established by the fiducial marks (Woltring et al., 1985; Yuan et al., 1997). In practice, bead measurement requires the definition of a small region-of-interest around each bead, and a DICOM image requires an annotation area on both top and bottom; for these reasons, we placed the beads with 50 mm setback from the long edge and 55 mm from the short one. Similarly, the control points were also placed peripherally. However, the reason for such placement is mainly to avoid overlapping between the control points and object points in the acquired image. From the measurement point of view, peripheral placement of fiducial marks and control points avoids overlap with object points, facilitating automatic marker detection and measurement.

After bead placements were determined, the bead spacing was investigated by numerical simulation under two spacing types: equal bead spacing with different bead number along the short and long side of the rectangular pattern, and different bead spacing with equal bead number along both sides. Considering both fiducial marks and control points, totally, four combinations were calculated, with 64 beads involved in each plane.

The influence of bead number (i.e. fiducial marks and control points) was finally investigated by numerical simulation. Four sets of bead number were considered to determine the optimal number in practice, from 8 beads, 16, 32 to 64 beads, where the smallest number is based on the usage of commercial calibration cages.

2.2.3 Computer synthetic image

Numerical simulation is very computationally efficient, but has limitations in its ability to replicate the reality of the RSA examination. To verify the derived parameters

that are also optimal under realistic circumstances, we developed a computer synthetic image technique that mimicked the factors of X-ray focal spot, exposure energy, and image noise. The technique was also applied to two widely used clinical cage systems, i.e. a uniplanar cage (cage 43 in UmRSA or UmeaHip in CMS-RSA) and a biplanar cage (Cage 10 or LundKnee); with the aim of comparing these cage systems with the current design.

The principle of image simulation, described in detail below, is based on a ray-tracking technique combined with the X-ray attenuation law, and an image degeneration method. First, the grey values of projected markers on a radiograph were acquired by simulating the RSA perspective projection and applying the X-ray attenuation law. Image degradation was then applied to mimic image blur, scattering, and noise.

2.2.3.1 Ray-tracking technique and X-ray attenuation law

Fundamental to X-ray image simulation is the ray-tracking technique and X-ray attenuation law (Duvauchelle et al., 2000). The ray tracking technique was applied by mimicking the X-ray perspective projection when a knee joint phantom was virtually placed in the calibration cage, using the same placement geometry as the numerical simulation. The positions of the focal spot and cage markers, as well as spherical marker sizes (Ø = 1.0 mm) and material (tantalum), were selected to be consistent with subsequent phantom studies. The penetration length of an X-ray beam through a spherical marker, corresponding to each image pixel, was calculated and converted to image gray scale value according to Beer's X-ray attenuation law (Duvauchelle et al., 2000).

$$N = N_0 e^{-\mu d} \qquad \text{(Equation 2.1)}$$

where N_0 is the number of incident X-ray photons; μ is the Linear Attenuation Coefficient (LAC) of the attenuating material; d is the path length; and N is the number of photons incident on the detector. The incident X-ray photon number N_0 was determined by the X-ray exposure parameters (Birch et al., 1979), which were chosen to

mimic subsequent phantom studies (as described in section 2.5). The LAC for tantalum was estimated for both 50 kVp exposures (mean energy = 30.2 keV) and 70 kVp exposures (mean energy = 38.2 keV); the LAC was 36 mm^{-1} and 20.5 mm^{-1}, respectively (Hubbell and Seltzer, 2004). The exit photon number N was then converted to 10-bit image gray scale level by assuming a linear relationship between image detector response and exit photon number (Duvauchelle et al., 2000).

2.2.3.2 Image degradation

The synthetic image generated by the previous procedure is an idealized version of a clinical radiograph. Generally, a clinical image is degraded by factors related to focal-spot blur, scattering and noise. (Bushberg, 2002). In practice, it is extremely complex to simulate the entire degradation. Therefore, we simplified the simulation procedure by modeling the degradation in the spatial domain as (Gonzalez et al., 2004):

$$g(x, y) = h(x, y) * f(x, y) + \eta(x, y) \qquad \text{(Equation 2.2)}$$

where f(x, y) is an ideal input pure image, '*' indicates convolution, h(x, y) is a linear, space-invariant Point Spread Function (PSF), and η(x, y) represents additive noise. We estimated the PSF by a blind deconvolution algorithm (Gonzalez et al., 2004), which used an iterative approach to estimate the Gaussian-distributed PSF that best characterizes the observed image blur. In our case, the algorithm, implemented in Matlab, returned a PSF that was described by a 2-D Gaussian distribution over a 5 x 5 matrix, with $\sigma = 0.83$ pixels. Noise in the image is also represented by a Gaussian distribution (Duvauchelle et al., 2000), with standard deviation similar to that found in phantom studies, using a modified average method (Olsen, 1993).

2.2.3.3 Implementation

The entire image simulation procedure was implemented in Matlab (The Mathworks Inc., MA, USA), with parameters selected to be consistent with subsequent phantom tests. These parameters included: image matrix dimension, detector element

spacing, gray scale discretization, X-ray focal spot location, cage location and marker geometry, and the location of the test object.

2.2.4 Phantom validation

A knee joint phantom was constructed and used in experimental comparison among cage systems. The phantom consists of a polymethyl methacrylate (PMAA) base, a 3-D translation positioning stage with accuracy of 2-μm reported by the manufacturer (Model M4434, Parker Hannifin Corp., PA, USA), a solid foam femur and a tibia (Sawbones, Pacific Research Labs, WA, USA). The femur was fixed on the base and the tibia was rigidly attached to the positioning stage. Sixteen tantalum beads (Ø = 1.0 mm) were inserted into the distal femur and proximal tibia, with 8 beads for each to construct RSA segments. The midpoint between the femoral and tibial components was placed close to the optimal position of the cage systems, as shown in Fig. 2.1. Clinical RSA configurations were mimicked with an X-ray source-to-image distance (SID) of 140 cm and 40 degrees between the two X-ray beams for the uniplanar cage; these values changed to 100 cm SID and 90 degrees for the biplanar cage. For the new cage, a SID of 160 cm and 90 degrees was used to represent biplanar parameters.

Two sets of phantom motion increments were applied, corresponding to the study of accuracy and precision (Önsten et al., 2001; Madanat et al., 2005; Mäkinen et al., 2005). For the precision part, zero motion between femur and tibia was used and radiographic exposures were repeatedly taken 12 times. To characterize accuracy, 16 random translation increments were performed along Y (proximal-distal), X (medial-lateral), and Z (anterior-posterior) axes, respectively. The increments applied are pre-calculated, based on a uniform distribution over the range of 0.02 – 1.73 mm. This motion range is similar to what has been used previously to mimic clinical procedures (Önsten et al., 2001; Bragdon et al., 2002; Börlin et al., 2006).

The exposure parameters were estimated from previous phantom studies (Önsten et al., 2001; Allen et al., 2004; Mäkinen et al., 2004; Ioppolo et al., 2007) and selected as 70 kVp at 16 mAs for both the new cage and the uniplanar cage, and 50 kVp at 4mAs for the biplanar cage. The radiographic examinations were performed in a dedicated RSA lab with two ceiling-mounted X-ray units (Proteus XR/a, GE Medical Systems, Milwaukee,WI, USA) and digital images were acquired by a computed radiography digital X-ray system (Capsula X CR, FujiFilm, Tokyo, Japan), which provides 3520 × 4280 image matrix for a 35 × 43 cm cassette and 2364 × 2964 matrix for a 24 × 30 cm cassette. Resulting digital images have 0.1-mm pixel spacing and 10-bit gray scale level.

In this study, all images were measured by commercial RSA analysis software (UmRSA Digital Measure® V2.2.1, RSA Biomedical, Umeå, Sweden) to determine marker locations. The two-dimensional measured marker locations were imported into an in-house RSA computation program for the computation of 3-D marker reconstructions and motion calculations (Yuan et al., 1997; Yuan and Ryd, 2000). The independent motion between femur and tibia was calculated from every two sequential image measurements. In total, six zero-motion situations and 8 motion increments were investigated for each cage. The relative motion has six degrees-of-freedom, with three rotations and three translations. In the RSA calculation, all translation components are calculated in combination with the rotation components (Selvik, 1989; Söderkvist and Wedin, 1993), but rotation components are less sensitive to errors than translation ones (Yuan et al., 1997). Therefore, in our study, only the translation components were evaluated.

2.2.5 Evaluation of precision and accuracy

Numerical simulation and computer-synthetic images provided the capability to estimate precision of our cage design prior to fabrication. Precision was evaluated along the X, Y, and Z axes, for the new cage and for previous biplanar and uniplanar designs. Precision was calculated as the standard deviation of repeated simulations, under

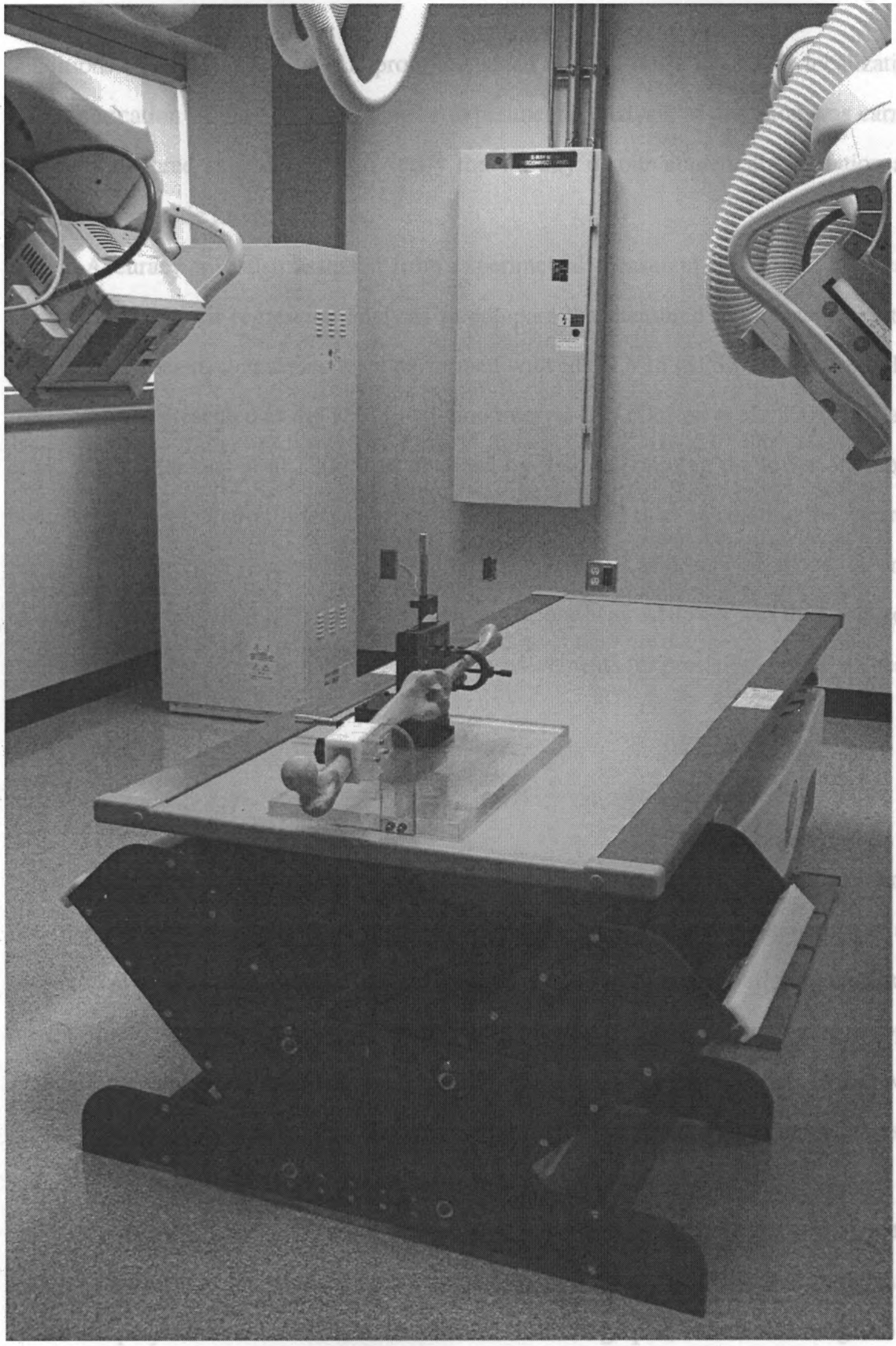

Figure 2.1 Illustration of the biplanar RSA system configuration for phantom experiments, with the new cage.

conditions of zero motion, with appropriate added random noise in marker localization. After fabrication of the new cage, similar experimental analysis of precision was carried out with all three cage designs, to verify the validity of our numerical simulation and computer-synthetic image analyses.

Accuracy was also assessed from experimental measurements on all three cage designs, using linear-regression analysis to compare the measured motion with the true increments. Statistical analyses were performed with SPSS V15 (SPSS Inc, Chicago, IL). Accuracy was presented as the 95% prediction interval (PI) (Önsten et al., 2001; Madanat et al., 2005; Mäkinen et al., 2005) as obtained by first determining the lower and upper bounds for the prediction interval for each observation and then calculating the mean of the intervals for each observation. Precision was calculated as described above. In order to address the statistical difference between cages, one-way ANOVA was then applied to the PI data sets for accuracy and the repeated measurements for precision, with P values of < 0.01 deemed significant.

2.3 Results

Among all previously defined calibration cage configurations, our analysis shows that the biplanar setup referred to as LundKnee possesses the highest accuracy and precision (Fig. 2.2), indicating that the biplanar setup is a superior configuration. Based on this fact, the new cage system was configured as a biplanar setup with an open structure corresponding to the large size of 35 × 43 cm film/image cassettes. In this way, the new cage configuration is applicable for any anatomic joints under any ranges of motion.

With respect to marker bead distribution, both image simulation and phantom tests confirmed that the bead placements were applicable to the clinical setting, i.e. all beads are projected within the field of view of the radiographs, as shown in Fig. 2.3. In addition, bead spacing was found to have negligible influence on the over-all RSA

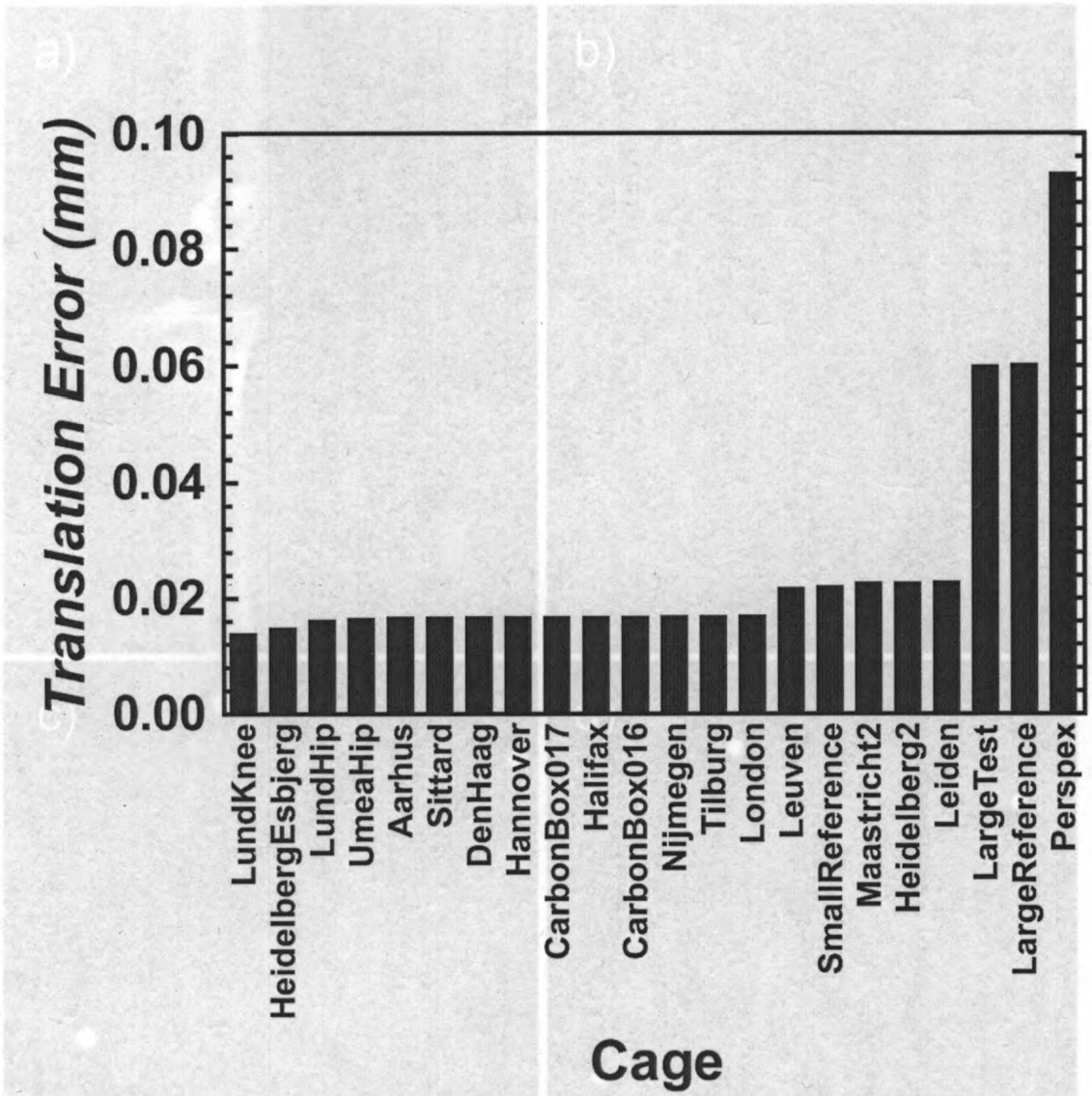

Figure 2.2 Comparison of numerical simulations for different cages, assuming the same error matrix with zero mean and 0.01 mm standard deviation. The resultant translation error was used as an outcome figure of merit.

accuracy and precision, as the maximum difference among four spacing combinations was less than 0.01 μm. Due to the different function of fiducial marks and control points, a different strategy was used with respect to the spacing and number. For fiducial marks, an equal number of beads was used on both long and short sides of the rectangular pattern, while control points were configured with equal spacing on both sides. Numerical simulations of bead number indicated that RSA precision is proportional to bead number, as shown in Fig. 2.4. However, 64 fiducial marks and control points

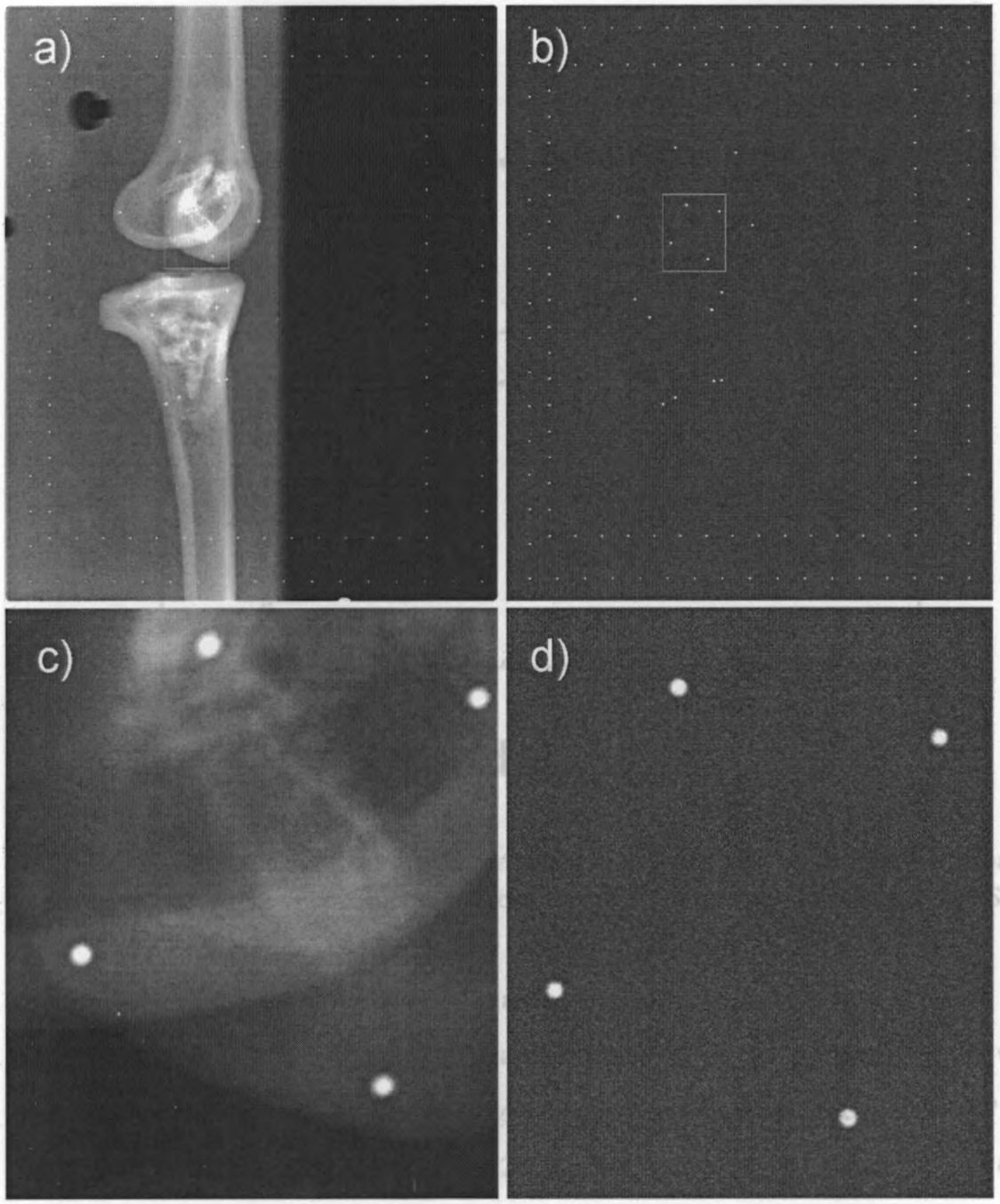

Figure 2.3 Illustration of a digital X-ray image of the phantom during testing of the new cage (a), compared to a computer-synthetic image of the same configuration (b). Image (c) and (d) represent magnified views of the region of interest identified in (a) and (b), respectively.

provided sufficient accuracy and precision in practice, with little gain expected beyond this number. Therefore in our design, we used 64 fiducial marks and 64 control points.

The final cage design (Fig. 2.5a) was fabricated as two compartments, each one with dimensions of 460 × 380 × 208 mm, with a fiducial plane at the bottom and a

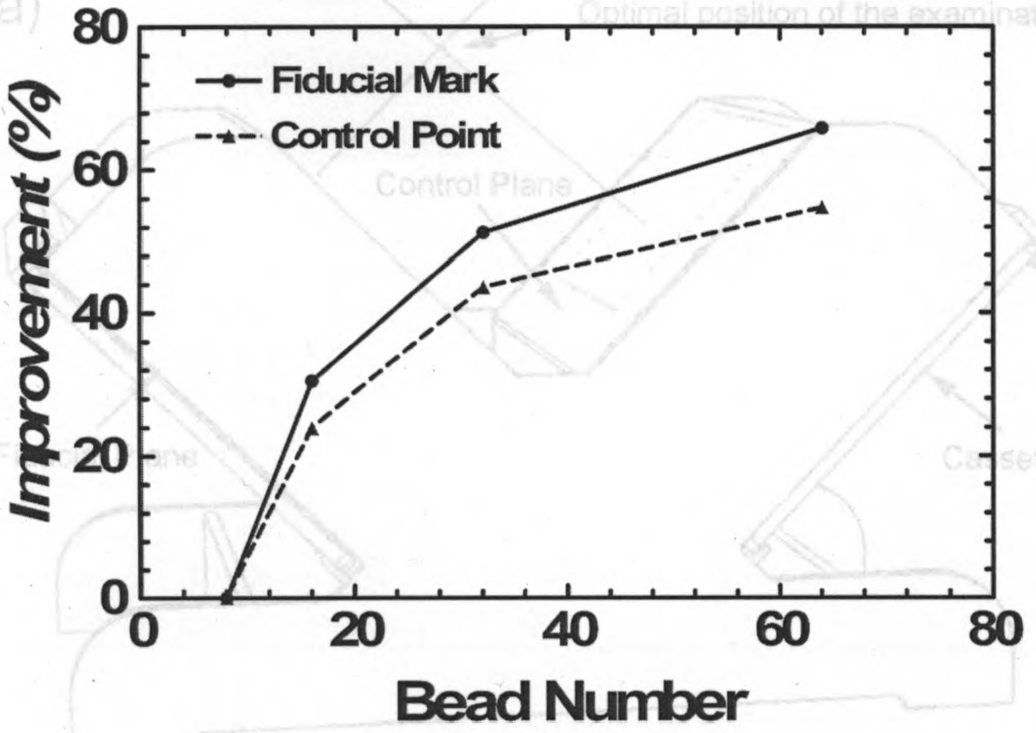

Figure 2.4 Results of numerical simulation, showing the improvement in precision that results from increasing the number of fiducial marks and control points of the new RSA cage design.

control plane at the top. The imaging planes were symmetrically placed at ± 45° with respect to vertical. The 64 spherical tantalum control points (Ø = 1.0 mm) were positioned in a 300 × 233.34 mm rectangular pattern with marker spacing of 16.67 mm along both the long and short sides (Fig. 2.5b). Correspondingly, 64 fiducial marks (Ø = 1.0 mm) were set in a 400 × 320 mm rectangular pattern, with a marker spacing of 25 mm in the long side and 20 mm in the short side (Fig. 2.5c).

Both numerical simulation and computer-synthetic image analysis predicted improved precision for the new cage design prior to fabrication (Table 2.1). The analysis also shows similar precision in all three directions for the new cage, while previous designs exhibit reduced precision in the X and Z directions, which involve out-of-plane localization. Also included in Table 2.1 are values of precision determined by

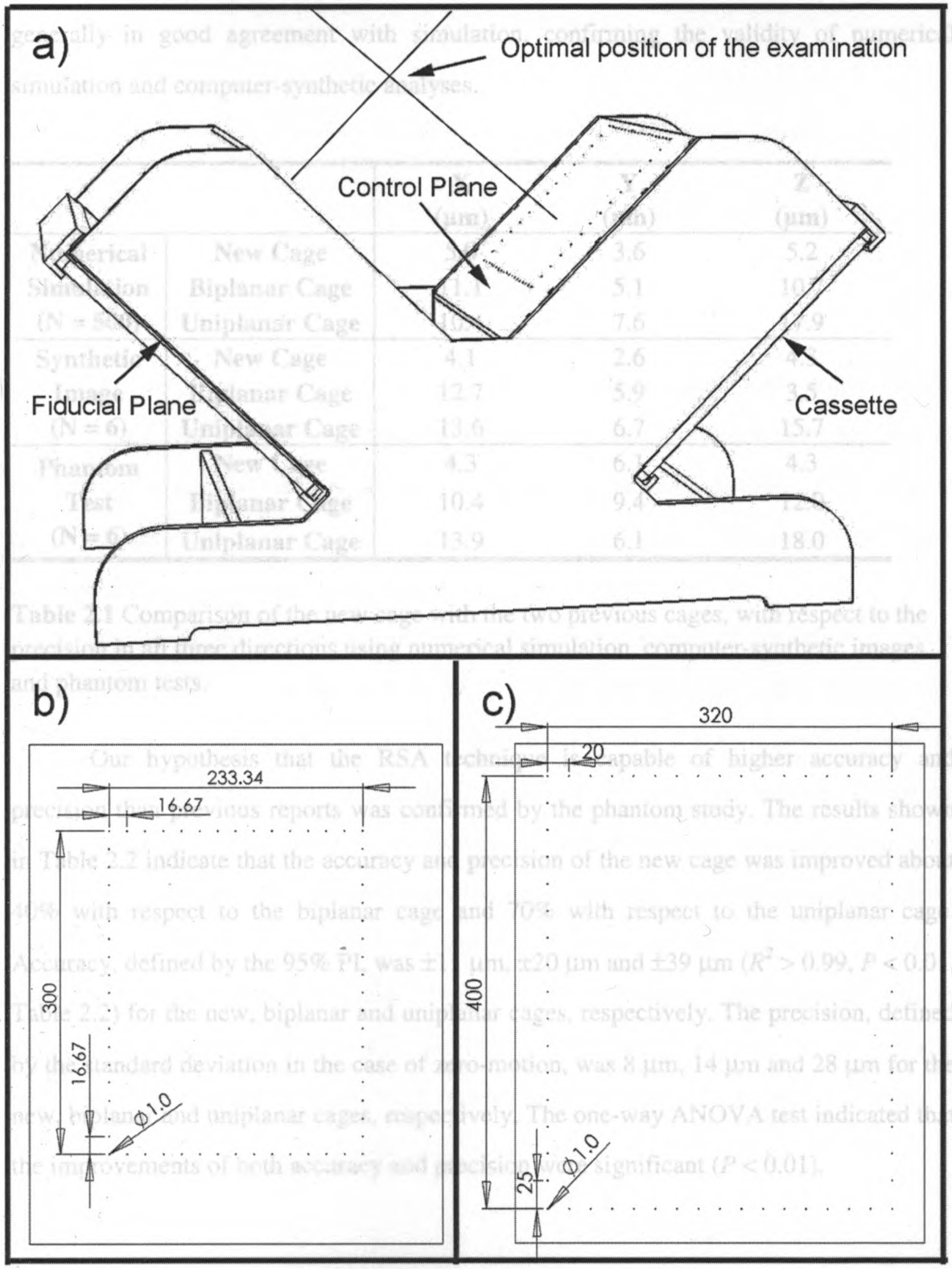

Figure 2.5 Schematic illustration of the enhanced biplanar calibration cage (a) and its bead configurations on both control (b) and fiducial (c) planes.

experimental measurements on our phantom. Experimentally determined precision was generally in good agreement with simulation, confirming the validity of numerical simulation and computer-synthetic analyses.

		X (μm)	Y (μm)	Z (μm)
Numerical Simulation (N = 500)	**New Cage**	5.0	3.6	5.2
	Biplanar Cage	11.1	5.1	10.7
	Uniplanar Cage	10.4	7.6	17.9
Synthetic Image (N = 6)	**New Cage**	4.1	2.6	4.3
	Biplanar Cage	12.7	5.9	3.5
	Uniplanar Cage	13.6	6.7	15.7
Phantom Test (N = 6)	**New Cage**	4.3	6.1	4.3
	Biplanar Cage	10.4	9.4	12.0
	Uniplanar Cage	13.9	6.1	18.0

Table 2.1 Comparison of the new cage with the two previous cages, with respect to the precision in all three directions using numerical simulation, computer-synthetic images, and phantom tests.

Our hypothesis that the RSA technique is capable of higher accuracy and precision than previous reports was confirmed by the phantom study. The results shown in Table 2.2 indicate that the accuracy and precision of the new cage was improved about 40% with respect to the biplanar cage and 70% with respect to the uniplanar cage. Accuracy, defined by the 95% PI, was ±11 μm, ±20 μm and ±39 μm ($R^2 > 0.99$, $P < 0.01$, Table 2.2) for the new, biplanar and uniplanar cages, respectively. The precision, defined by the standard deviation in the case of zero-motion, was 8 μm, 14 μm and 28 μm for the new, biplanar and uniplanar cages, respectively. The one-way ANOVA test indicated that the improvements of both accuracy and precision were significant ($P < 0.01$).

	Accuracy[a] (95% prediction interval in μm)	Precision (SD of zero motion in μm)
New Cage	±11	8
Biplanar Cage	±20	14
Uniplanar Cage	±39	28

[a] For each linear regression equation $R^2 > 0.99$ and $P < 0.01$

Table 2.2 Experimental comparison of accuracy and precision between the new, biplanar, and uniplanar cages.

2.4 Discussion

We report a new calibration cage design, which significantly improves the accuracy and precision of RSA, compared to existing clinical systems. Optimization of the number of marker beads, the bead placement, and the configuration of the imaging planes all contributed to the observed improvement, which was confirmed by two types of simulation and by experimental measurements with a phantom.

Accuracy and precision reported in this study represents performance under idealized radiographic conditions (i.e. 50 – 70 kVp and reduced scatter without soft tissue). In practice, accuracy and precision are not expected to reach the levels reported in Table 2.2. Nonetheless, the relative performance of different cage designs should be indicated reliably by our study. It is reasonable to expect the new cage to perform with approximately twice the reported precision and accuracy of existing clinical cages (Kärrholm, 1989; Vrooman et al., 1998; Börlin et al., 2002). In this case, we could expect that the accuracy and precision of the optimized RSA system will approach ± 55μm in clinical implementation. However, it should be pointed out that further validation under clinical situations, which mimic error sources introduced by the patient, are required before it can be recommended for future clinical studies.

Acknowledgements:

The authors gratefully acknowledge the assistance of the machine shop, University of Western Ontario for the new cage fabrication. This work was supported by the Canadian Institutes of Health Research (CIHR) and National Research Council of Canada (NRC).

2.5 References

Allen, M. J., Hartmann, S. M., Sacks, J. M., Calabrese, J., Brown, P. R., 2004. Technical feasibility and precision of radiostereometric analysis as an outcome measure in canine cemented total hip replacement. Journal of orthopaedic science 9(1), 66-75.

Birch, R., Marshall, M., Ardran, G. M., 1979. Catalogue of Spectral Data For Diagnostic X-rays. The Hospital Physicists' Association.

Börlin, N., Röhrl, S. M., Bragdon, C. R., 2006. RSA wear measurements with or without markers in total hip arthroplasty. J Biomech 39(1641-50).

Börlin, N., Thien, T., Kärrholm, J., 2002. The precision of radiostereometric measurements. Manual vs. digital measurements. J Biomech 35(1), 69-79.

Bragdon, C. R., Malchau, H., Yuan, X., Perinchief, R., Kärrholm, J., Börlin, N., Estok, D. M., Harris, W. H., 2002. Experimental assessment of precision and accuracy of radiostereometric analysis for the determination of polyethylene wear in a total hip replacement model. J Orthop Res 20(4), 688-95.

Bushberg, J. T., 2002. The essential physics of medical imaging. Lippincott Williams & Wilkins, Philadelphia.

Choo, A. M., Oxland, T. R., 2003. Improved RSA accuracy with DLT and balanced calibration marker distributions with an assessment of initial-calibration. J Biomech 36(2), 259-64.

Dalen, T., Nilsson, K. G., 2005. VersaBond bone cement prospective randomized study of the clinical properties of a new bone cement in total knee replacement. Knee 12(4), 311-7.

Digas, G., 2005. New polymer materials in total hip arthroplasty. Evaluation with radiostereometry, bone densitometry, radiography and clinical parameters. Acta Orthop Suppl 76(315), 3-82.

Digas, G., Karrholm, J., Thanner, J., Malchau, H., Herberts, P., 2003. Highly cross-linked polyethylene in cemented THA: randomized study of 61 hips. Clin Orthop Relat Res(417), 126-38.

Digas, G., Kärrholm, J., Thanner, J., Malchau, H., Herberts, P., 2004. The Otto Aufranc Award. Highly cross-linked polyethylene in total hip arthroplasty: randomized evaluation of penetration rate in cemented and uncemented sockets using radiostereometric analysis. Clin Orthop Relat Res(429), 6-16.

Duvauchelle, P., Freud, N., Kaftandjian, V., Babot, D., 2000. A computer code to simulate X-ray imaging techniques. Nuclear Instruments and Methods in Physics Research Section B: Beam Interactions with Materials and Atoms 170(1-2), 245-258.

Garling, E. H., Kaptein, B. L., Geleijns, K., Nelissen, R. G., Valstar, E. R., 2005. Marker Configuration Model-Based Roentgen Fluoroscopic Analysis. J Biomech 38(4), 893-901.

Gonzalez, R. C., Woods, R. E., Eddins, S. L., 2004. Digital Image processing using MATLAB. Pearson Prentice Hall, Upper Saddle River, N. J.

Hubbell, J. H., Seltzer, S. M., 2004. Tables of X-Ray Mass Attenuation Coefficients and Mass Energy-Absorption Coefficients (version 1.4). [Online] Available: http://physics.nist.gov/xaamdi [2007, June 27]. National Institute of Standards and Technology, Gaithersburg, MD.

Ioppolo, J., Borlin, N., Bragdon, C., Li, M., Price, R., Wood, D., Malchau, H., Nivbrant, B., 2007. Validation of a low-dose hybrid RSA and fluoroscopy technique: Determination of accuracy, bias and precision. J Biomech 40(3), 686-92.

Kärrholm, J., 1989. Roentgen stereophotogrammetry. Review of orthopedic applications. Acta Orthop Scand 60(4), 491-503.

Kärrholm, J., Borssen, B., Lowenhielm, G., Snorrason, F., 1994. Does early micromotion of femoral stem prostheses matter? 4-7-year stereoradiographic follow-up of 84 cemented prostheses. J Bone Joint Surg Br 76(6), 912-7.

Kärrholm, J., Herberts, P., Hultmark, P., Malchau, H., Nivbrant, B., Thanner, J., 1997. Radiostereometry of hip prostheses. Review of methodology and clinical results. Clin Orthop Relat Res(344), 94-110.

Madanat, R., Makinen, T. J., Moritz, N., Mattila, K. T., Aro, H. T., 2005. Accuracy and precision of radiostereometric analysis in the measurement of three-dimensional micromotion in a fracture model of the distal radius. J Orthop Res 23(2), 481-8.

Mäkinen, T. J., Koort, J. K., Mattila, K. T., Aro, H. T., 2004. Precision measurements of the RSA method using a phantom model of hip prosthesis. J Biomech 37(4), 487-93.

Mäkinen, T. J., Mattila, K. T., Määttänen, H., Aro, H. T., 2005. Comparison of digital and conventional radiostereometric image analysis in an ankle phantom model. Scand J Surg 94(3), 233-8.

McCalden, R. W., Naudie, D. D., Yuan, X., Bourne, R. B., 2005. Radiographic methods for the assessment of polyethylene wear after total hip arthroplasty. J Bone Joint Surg Am 87(10), 2323-34.

Olsen, S., 1993. Noise Variance Estimation in Images. In the 8th Scandinavian Conference on Image Analysis. Tromsø, Norway.

Önsten, I., Berzins, A., Shott, S., Sumner, D. R., 2001. Accuracy and precision of radiostereometric analysis in the measurement of THR femoral component translations: human and canine in vitro models. J Orthop Res 19(6), 1162-7.

Röhrl, S. M., Nivbrant, B., Strom, H., Nilsson, K. G., 2004. Effect of augmented cup fixation on stability, wear, and osteolysis: a 5-year follow-up of total hip arthroplasty with RSA. J Arthroplasty 19(8), 962-71.

Ryd, L., 1986. Micromotion in knee arthroplasty. A roentgen stereophotogrammetric analysis of tibial component fixation. Acta Orthop Scand Suppl 220, 1-80.

Ryd, L., Yuan, X., Lofgren, H., 2000. Methods for determining the accuracy of radiostereometric analysis (RSA). Acta Orthop Scand 71(4), 403-8.

Selvik, G., 1989. Roentgen stereophotogrammetry. A method for the study of the kinematics of the skeletal system. Acta Orthop Scand Suppl 232, 1-51.

Selvik, G., 1990. Roentgen stereophotogrammetric analysis. Acta Radiol 31(2), 113-26.

Söderkvist, I., Wedin, P. Å., 1993. Determining the movements of the skeleton using well-configured markers. J Biomech 26(12), 1473-7.

Valstar, E. R., Vrooman, H. A., Toksvig-Larsen, S., Ryd, L., Nelissen, R. G., 2000. Digital automated RSA compared to manually operated RSA. J Biomech 33(12), 1593-9.

Vrooman, H. A., Valstar, E. R., Brand, G. J., Admiraal, D. R., Rozing, P. M., Reiber, J. H., 1998. Fast and accurate automated measurements in digitized stereophotogrammetric radiographs. J Biomech 31(5), 491-8.

Woltring, H. J., Huiskes, R., de Lange, A., Veldpaus, F. E., 1985. Finite centroid and helical axis estimation from noisy landmark measurements in the study of human joint kinematics. J Biomech 18(5), 379-89.

Yuan, X., Ryd, L., 2000. Accuracy analysis for RSA: a computer simulation study on 3D marker reconstruction. J Biomech 33(4), 493-8.

Yuan, X., Ryd, L., Blankevoort, L., 1997. Error propagation for relative motion determined from marker positions. J Biomech 30(9), 989-92.

3 Development of an automatic measurement program for RSA radiographs

3.1 Introduction

RadioStereometric Analysis (RSA) has been proven to be the most accurate three-dimensional (3-D) *in vivo* measurement tool in orthopaedic studies (Kärrholm, 1989; Kärrholm et al., 1997; McCalden et al., 2005). However, its large-scale clinical applications are limited by its complexity and the expertise required for its use. In general, RSA procedures include synthetic landmark insertion, stereoradiographic examination, radiographic measurement, and the final data analysis. The problems of the complex and time-consuming procedures are mainly caused by the radiographic measurement, i.e. two-dimensional (2-D) measurement, of markers in RSA radiography. This process, consisting of marker detection, marker centroid refining, and marker identification, was conducted manually before the late 1990's. Investigators needed to be trained to detect, refine and identify each marker in the 2-D radiology image. Using the manual approach, approximately one hour is required per RSA radiograph (Vrooman et al., 1998).

Much work has been done to make this measurement procedure more user-friendly, including conversion from manual to digital processes, and the development of semi- or fully automatic digital measurement programs (Ostgaard et al., 1997; Vrooman et al., 1998; Olsson, 2001; Börlin et al., 2002; Thistlethwaite, 2002). All of these improvements have significantly reduced the complexity and time consumption of RSA.

However, there is still room for improvement in the existing software, in terms of user-friendliness, accuracy and precision. Currently, three software packages are available on the market, UmRSA® (Biomedical Innovations AB, Umeå, Sweden), RSA-CMS® (MEDIS Medical Imaging Systems VB, Leiden, the Netherlands), and WinRSA (Tilly Medical Products AB, Lund, Sweden). Two of these, the UmRSA and

RSA-CMS, are now widely utilized in RSA studies. The UmRSA system has shown better accuracy and precision than RSA-CMS (Bragdon et al., 2004), but it is a semi-automatic program, and a certain level of RSA knowledge is required to operate the software. While RSA-CMS is fully automatic, it has poorer performance, and many interactive corrections may be needed after the automated process. In addition, both of these programs are not able to support fully automated measurement of radiography taken with our newly designed calibration cage (See Chapter 2). This means that the measurement of RSA radiography produced by the novel cage must be carried out manually. This becomes a serious problem, because there are 256 cage markers in the enhanced calibration system and, using the UmRSA program, 30 minutes per pair of images is required.

Recently, the progress of computing power and digital image processing techniques has made it possible to improve the measurement procedure. To achieve our goals, we compared and modified the major algorithms for RSA radiographic measurement, including steps of marker detection, centroid refining and identification, and implemented the most advantageous ones. The program, which we refer to as Automated Fitting and Identification - RSA (AFI-RSA), eliminates the majority of user interaction, is able to support the new calibration cage, and has comparable accuracy and precision to commercial RSA measurement programs.

3.2 Methods

Matlab (The Mathworks Inc., MA, USA) has been employed as the main tool to develop the measurement program of RSA radiography (Börlin et al., 2002; Thistlethwaite, 2002). In this project, AFI-RSA was developed and implemented in Matlab 7.0 R14 on a Mobile Intel P4 3.33 GHz, 1 G RAM computer. Each step of this program development will be discussed in the following sections.

3.2.1 Image Enhancement

Performance of RSA measurement largely depends on the quality of the radiograph. To maximize the outcome, image quality needs to be improved prior to analysis. Typical image enhancements consist of noise reduction, as well as intensity and histogram adjustment. Noise in a radiograph can be simply represented by a Gaussian distribution (Duvauchelle et al., 2000; Gravel et al., 2004). To remove noise, we utilized 2-D adaptive Wiener noise-removal filtering, which is usually used to reduce Gaussian noise and preserve important edges and other high-frequency structures. In some cases, the contrast between the marker and its background is very low. This makes it difficult to find markers in the marker detection stage. Intensity and histogram adjustment can be utilized to improve image contrast significantly, but this modifies the gray values, possibly affecting the marker centroid detecting results (Fig. 3.1). In consideration of this possibility, intensity and histogram adjustment are not employed in our program. The final results actually show that AFI-RSA is able to find markers under complex backgrounds, even though no intensity or histogram adjustment was utilized.

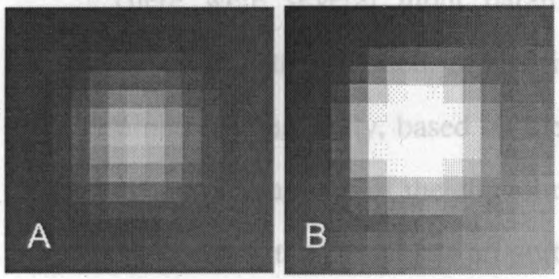

Figure 3.1 Marker image before and after histogram adjustment. A, The original image, the center could be detected easily; B, After histogram adjustment, the marker center is blurred.

3.2.2 Marker Detection

The next step in automatic RSA measurement is to find potential markers in the radiograph. This is an important step due to the fact that the marker centroid refining and identifying procedures are based on the results of this step. The detection rate, which is

defined as the number of markers found divided by the number of markers which exist, should be as high as possible.

In the step of marker detection, several automated algorithms have been reported, including: 1. Edge detection followed by Hough transform (Vrooman et al., 1998); 2. Convolution with a kernel-on-edge detected image (Thistlethwaite, 2002); 3. Gray-scale opening (Olsson, 2001); and 4. Convolution with a Mexican Hat Filter (MHF) (Buck et al., 2003). The first two methods have been evaluated, with method 2 showing significant advantages over method 1 (Thistlethwaite, 2002). However, there have not yet been any comparisons made between methods 2, 3, and 4. In order to utilize the best approach in our program, we have implemented each algorithm. We used 10 pairs of RSA phantom images (1760 x 2140 pixels, 14 x 17 inches) for testing; each image had markers in different sizes and backgrounds.

There were several input parameters which needed to be defined for each algorithm before getting started. In algorithm 2, the threshold of the Sobel edge detector is determined automatically, based on the mean of the gradient magnitude in the image. The fixed central diameter of the convolution kernel is 8 pixels, and its response range is 3 pixels. Therefore, the kernel has proportional responses for markers which range in size from 2 to 14 pixels. The threshold of response for convolution results was chosen by trial and error, and applied to all testing images. Two factors needed to be determined in gray-scale opening. The size of the structural element was computed based on the geometric configuration of the RSA experiment. The maximum size of the projected marker in the radiograph was about 2 mm, or 10 pixels. Two pixels of blurring around the projected marker were added, where the value was acquired by studying real images. In summary, the size of the structural element was defined as 14 pixels, which means that all markers smaller than 14 pixels would be retrieved. The global threshold for finding potential markers is determined by trial and error. The size of MHF is one parameter which needs to be determined in the last algorithm. The kernel is specified for a marker

size of 8 pixels. After convolution, a global characteristic threshold used to distinguish possible markers from random noise, is also required (Buck et al., 2003).

3.2.3 Marker Centroid Refining

The approximate marker center is determined in the marker detection procedure, which is defined as the center of boundary box of the possible marker. It is not precise because image noise, distortion, and other factors might affect the size of the boundary box. This inaccuracy could be propagated in subsequent computations (Yuan, 2000). Therefore, marker centers need to be measured precisely. Meanwhile, the possible markers detected in the previous process consist of false hits; they should be excluded in this step. Several approaches have been developed for this purpose, including linear approximation of detected marker edge to a circle equation (Ostgaard et al., 1997), least-squares fitting of detected edge to an ellipse outline (Thistlethwaite, 2002), least-squares fitting of paraboloid to the gray value profile of the marker (Vrooman et al., 1998), and least-squares fitting of 3-D sigmoid model to the gray value profile of the marker (Börlin et al., 2002). The method of 3-D sigmoid model fitting has demonstrated outstanding performance and has been widely employed (Bragdon et al., 2004). We then choose to utilize the 3-D model fitting in our program.

3.2.3.1 Models

The problem of marker centroid refining can be depicted as a weighted non-linear least squares optimization problem as follows (Börlin et al., 2002):

$$\min_{\theta} \sum_{(x,y)\in S} W(x,y)(f(x,y;\theta)-i(x,y))^2 \qquad \text{(Equation 3.1)}$$

where i(x, y) is the image gray value of a pixel (x, y), W(x, y) is a weight function, S is the region of interest (ROI) in the image, and f(x, y, θ) is a model function with the parameter set θ. The problem is solved by finding the optimal parameter set θ using iterative fitting. The marker center in θ is then determined as the final solution. Based on

a survey of markers in clinical images, structures in RSA radiography are categorized into three types of models: marker, gradient background, and edge (Börlin et al., 2002). Each model has the ability to represent the appropriate structure in a RSA image. Four composite models were then composed from these three structure models for fitting.

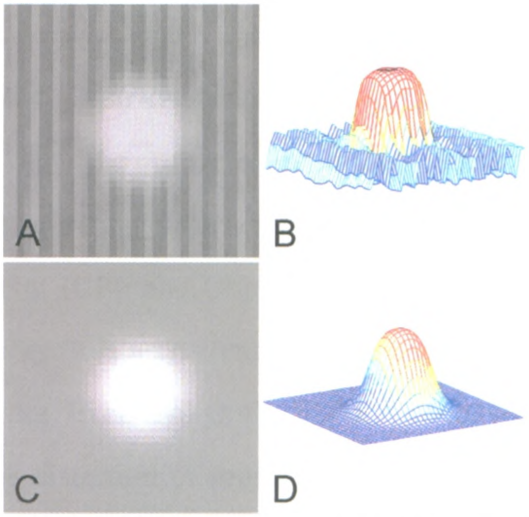

Figure 3.2 Illustration of marker model fitting. A and B show the image data of the single marker with noise background composite model. C and D show best model fit.

3.2.3.2 Fitting

The algorithm for fitting has been described completely (Börlin et al., 2002). The basic idea is to choose a composite model $f(x, y, \theta)$ in Equation 3.1, and then input an initial parameter set θ for non-linear least squares fitting. The marker center is obtained from the best fit results. The model fitting is illustrated in Fig. 3.2. We implemented the algorithm, but it is not perfectly user-friendly. To improve its efficiency, we have made several modifications to AFI-RSA.

The first improvement is in the way the composite model is chosen. In Börlin's algorithm, the model is determined manually, while an edge-detection algorithm is utilized before fitting in our program. If an edge is detected within the ROI, the model that is composed of a marker, background, and an edge will be used. Otherwise, the default model that consists of a marker and a background will be chosen. The procedure takes place without any user interaction. Since the other composite models, e.g. with two markers, a background, and an edge were rarely found in RSA radiography (Börlin et al., 2002), they have not been implemented in AFI-RSA.

In non-linear least squares fitting, the results largely depend on the initial parameter estimation. AFI-RSA uses the same way as in other studies (Olsson, 2001;

Börlin et al., 2002) to estimate most parameters, except for the edge profile parameter. The new method applies a 'Canny' edge detector to find all possible edges in the ROI, and fit each connected component to a linear function. The component that most closely approximates the line is chosen as the edge in the composite model, and the profile of the edge is determined based on the equation of that line.

3.2.4 Marker Identification

The process of marker identification consists of several tasks, including categorizing detected markers into different groups, i.e. Fiducial Mark (FM), Control Point (CP), and Object Point (OP), and numbering markers of each group in a specific order. It is a challenge to automatically identify each marker with a specified group and order. Even though the FM and CP have distinct distributions, the pattern is disturbed by the distortion of projection, the variety of detector orientations and sizes, measurement error, and overlapped markers. All of these factors complicate the recognition of markers of each group.

Börlin et al. introduced a semi-automatic identification method (Börlin et al., 2002). By measuring two or three FMs/CPs, or giving the positions of lead crosses on FM/CP planes, other markers in FM and CP can be discovered automatically. Several fully automatic approaches have been developed. The rectangular pattern of FM and CP markers was employed to distinguish them from OP (Vrooman et al., 1998; Olsson, 2001). However, some cages have a non-rectangular pattern of CP. Due to these exceptions, this method cannot be used to differentiate CP from OP. As for the methods used to distinguish FM from CP, several manners have been utilized, including matching the known layout of each group in order to recognize them (Vrooman et al., 1998), and separating them based on the different sizes of projected markers in each group (Olsson, 2001). The former technique has a limitation because some cages, e.g. the biplanar cage, have the same layout as FM and CP, which means they can not be divided in this manner.

We therefore developed a routine for the automated identification of RSA markers. The new algorithm is compatible with the novel cage described in Chapter 2 and the widely used uniplanar and biplanar cages from RSA Biomedical. The algorithm is based on the collinearity of cage markers. In this way, the pattern and layout of FM and CP no longer affect the identification. The steps can be described as follows:

- For each marker, m1, define a line between it and another marker, m2, where m2 is any one of all the markers except for m1. This step should generate *n-1* lines, where *n* is the total marker number.
- For each line, determine how many other markers are on it. Because of the deviation caused by measurement error, marker centers are not exactly collinear. This error is allowed and the threshold of deviation is defined as approximately half of the projected marker size.
- Record the maximum number of markers on the same line, and assign this number to the marker m1.
- Repeat steps 1 – 3 for each marker m_n.
- Since cage markers are collinear, they must have more markers than Object Points on a certain line. Cage markers can then be separated from Object Points.
- The CP and FM can now be divided by their sizes. The CPs are closer to the X-ray focus, so their sizes in the radiograph should be larger than the FMs (Olsson, 2001). The *n* largest markers are defined as CP, where *n* is the number of CP as determined by the cage type.
- Other markers left are identified as OPs.
- Markers in each group are numbered according to their related locations.

3.2.5 Phantom Study

To assess the performance of this newly developed program, a phantom study was conducted to compare it with two widely used commercial software applications, UmRSA Digital Measure® V2.2.1 (Börlin et al., 2002) and RSA-CMS® V4.3 (Vrooman et al., 1998). An *in vitro* phantom was constructed for this study; its details have been described in Chapter 2. The system set-up of the study is similar to the Phantom Validation in Chapter 2, except that only the uniplanar cage and the novel cage from Chapter 2 were employed in this study. Two X-ray machines were used (AMX4 Plus Portable X-ray system, GE Healthcare, USA and Digital-X 80HF, Fischer Imaging, USA) and the digital images were acquired by a computer radiography system (FCR XG-1, Fuji Photo Film Co., LTD, Tokyo, Japan).

A total of 28 radiograph pairs were acquired using the uniplanar cage, resulting in 14 independent RSA exams. For every exam-pair, we used the three programs (AFI-RSA, UmRSA, and RSA-CMS) to measure the 2-D coordinates of each marker in the radiograph. No user interaction was involved when using RSA-CMS and AFI-RSA, i.e. the user is only required to input the images and retrieve the results; the programs take care of all other procedures. For UmRSA, the operator needs to manually locate and number the cage and object markers. To compare measurement programs only and not the entire software packages, these 2-D coordinates were imported into an in-house mathematic routine (Yuan et al., 1997; Yuan and Ryd, 2000) that was implemented in Matlab to reconstruct 3-D marker positions and compute relative motions. Only the resulting translation components of the motion were evaluated.

The accuracy of all three programs was assessed using linear-regression analysis, to compare the measured motions with their true increments. Accuracy was presented as a 95% prediction interval (PI) (Önsten et al., 2001; Madanat et al., 2005; Mäkinen et al., 2005), as obtained by first determining the upper and lower bounds of the prediction interval, and then calculating the mean of the intervals for each observation. Precision

was calculated as the standard deviation of repeated measurements, under conditions of zero motion. To analyze the statistical differences between programs, a one-way Analysis of Variance (ANOVA) was used to test the PI data sets for accuracy and the repeated measurements for precision, with P values of < 0.01 deemed significant. Statistical analyses were performed with SPSS V15 (SPSS Inc, Chicago, IL).

The success rate of measurement, defined as the number of markers measured successfully and automatically over the number of markers which exist, was compared for the two fully automatic programs, RSA-CMS and AFI-RSA. This definition of successful measurement means that markers are located, centroid refined, and recognized in correct groups, i.e. FM, CP, or OP. Since UmRSA is semi-automatic, it is not necessary to evaluate the program for success rate of measurement.

In order to test the capacity of AFI-RSA to support the fully automated radiograph measurement taken with the newly developed cage, our in-house code was utilized to measure 28 pairs of radiographs, that were acquired with the new cage. The success rate of measurement was evaluated under similar conditions as the previous examination.

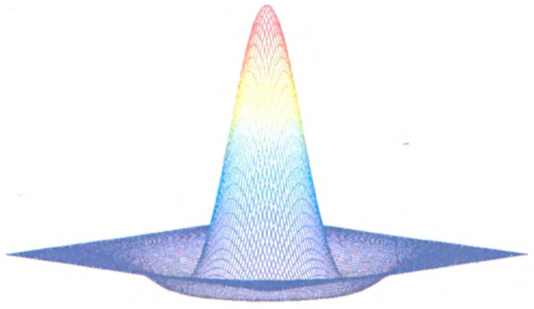

Figure 3.3 Mexican Hat Filter.

3.3 Results

The results of the comparison of marker detection algorithms are shown in Table 3.1. Time measurements were recorded for the time taken by the algorithm to process one pair of images. The input parameters were the number of factors that needed to be defined before running the experiment, which sometimes required manual adjustment for various sizes or backgrounds of images.

	Beads #	Detection Rate (%)	Time (s) Mean±SD	Input Parameters
Edge Detection+Convolution	1271	91.9	16.5±0.7	3
Gray-Scale Opening	1271	99.4	28.6±0.6	2
Convolution with MHF	1271	99.9	18.2±0.5	2

Table 3.1 Comparison of marker detection algorithms.

Based on these results, we decided to choose the convolution with MHF as the method for marker detection in our program. This novel approach applies the fact that the radiographic projection of a spherical marker is very similar to a Gaussian function in 2-D (Buck et al., 2003). The kernel is then constructed by applying a negative second derivative of the 2-D Gaussian function, which is also called the MHF, according to its shape (Fig. 3.3). Once the image is filtered, a characteristic threshold is sufficient to determine possible markers by identifying clusters which have gray-values higher than the threshold. This method has demonstrated a great success rate and time efficiency in high resolution digital images (Buck et al., 2003), but to the best of our knowledge, it has never been applied in the RSA measurement program. We used MHF in all subsequent results.

The results of comparison of programs indicate that the accuracy and precision of the new AFI-RSA program was comparable with the two extensively applied programs. Accuracy, defined by the 95% PI, was ± 45 μm, ±37 μm, and ±49 μm ($R^2 > 0.99$, $P < 0.01$) for the AFI-RSA, UmRSA, and RSA-CMS programs, respectively. Precision, defined by the standard deviation in the case of zero-motion, was 20 μm, 21 μm, and 22 μm for the AFI-RSA, UmRSA, and RSA-CMS programs, respectively. The one-way ANOVA test indicated that the difference in accuracy between the programs was significant ($P < 0.01$). No significant difference in precision was found between the three programs ($P = 0.36$).

The measurement success rate of RSA-CMS was 60.4%, compared with 91.4% for the in-house AFI-RSA code (Table 3.2), showing an improvement in user-friendliness of about 50%.

	Markers Exist	Measured Successfully	Success Rate
RSA-CMS	2688	1624	60.4%
AFI-RSA	2688	2456	91.4%

Table 3.2 Measurement success rate of the two automated programs with respect to radiographs taken with the uniplanar cage.

The measurement success rate of the AFI-RSA code was 96.3%, when applied to radiographs taken with the new cage (Table 3.3), showing the high capacity of AFI-RSA for supporting the new cage. Note that, no comparison with UmRSA or RSA-CMS was possible with respect to the new cage, due to the fact that these applications do not support novel cage geometry.

	Markers Exist	Measured Successfully	Success Rate
AFI-RSA	8064	7767	96.4%

Table 3.3 Measurement success rate of AFI-RSA, when applied to radiographs taken with the cage newly developed in Chapter 2.

3.4 Discussion

We have developed an enhanced measurement program for the RSA radiograph, which implements optimized algorithms and is fully automatic. The program can be utilized in RSA projects to improve user-friendliness and throughput significantly. When compared to the two widely used commercial software applications, this new program has equivalent precision and similar accuracy. In terms of user-friendliness, the new program requires less user interaction than UmRSA and has a higher measurement success rate than the most commonly used fully automatic program, RSA-CMS.

It was previously demonstrated that the performance of UmRSA is superior to RSA-CMS (Bragdon et al., 2004). However, no significant difference in precision between the two programs was found in the current study. This may be because different versions of the software were used for the studies. The version of RSA-CMS utilized in our project was V4.3, which was published after Bragdon's research. The program's precision may have been improved, making RSA-CMS more comparable to UmRSA.

For software development, computing speed should be fast. However, the measurement performance, including accuracy, precision and measurement success rate take priority over computing time. We believe that increasing computer power will keep improving the software speed in the future, but this is not the case for measurement performance. The typical time to process a pair of phantom images (3520 x 4280 pixels, 250 DPI) taken with uniplanar cage is about 10 minutes, using the in-house AFI-RSA code on the P4 3.33GHz machines described above. This takes less than 1 minute using RSA-CMS, due to its faster fitting algorithm. However, the measurement success rate of RSA-CMS is lower than AFI-RSA. This is a severe problem, because manual correction

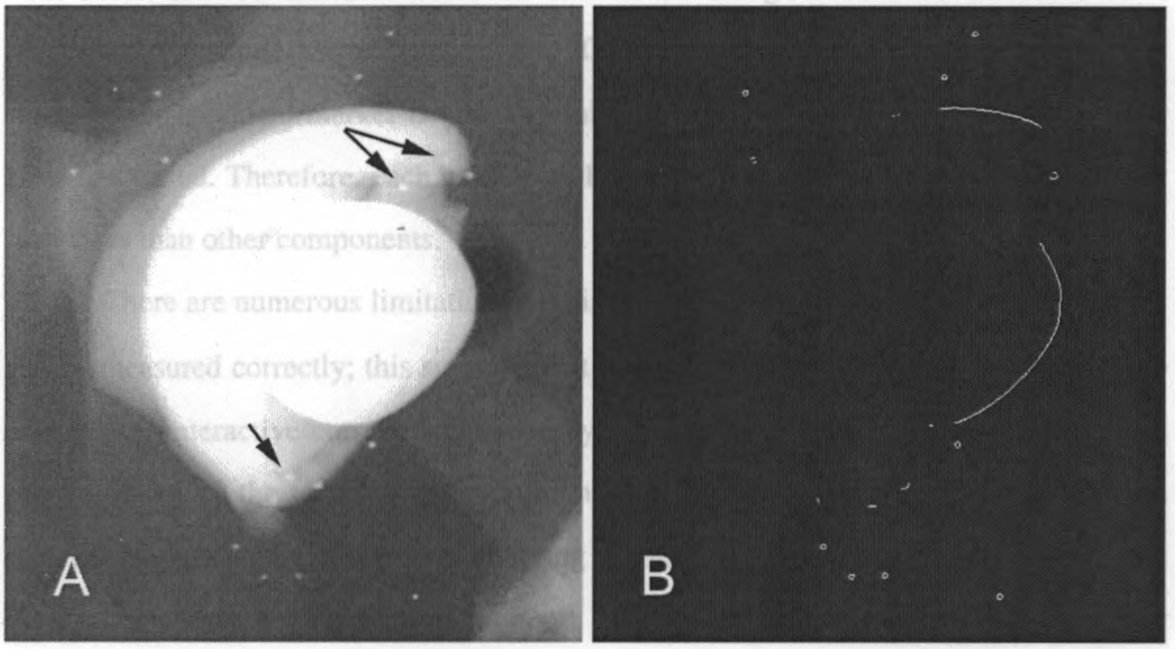

Figure 3.4 Problem of Sobel edge detector. A, Sample region of THR image; B, After applying the Sobel edge detector, most markers inside the femoral head and acetabular cup can't be detected (arrow).

of the measurement error is a time consuming process and requires considerably more effort. At the same time, the accuracy of RSA-CMS is significantly lower than AFI-RSA.

Edge Detection plus Convolution yields the worst results among the three approaches of marker detection, but a great outcome was reported when it was employed on Total Knee Replacement images (Thistlethwaite, 2002). By examining our images, we found that the problem was caused by edge detection. In areas with high intensity backgrounds, the Sobel edge detector failed to discover marker edges with its automatic threshold determining algorithm. Our testing images were from Total Hip Replacements (THR), and some Object Points overlapped with the femoral head and acetabular cup, which both have high intensities (Fig. 3.4). It may be helpful to tune the threshold manually when using edge detection, in order to obtain the needed edge information. However, only a small number of user interactions should be involved for an automated program. If a better method can be developed for determining the threshold of the Sobel detector, the algorithm may be acceptable. Canny edge detection is more effective than Sobel, but it is more time-consuming and brings in more disturbed noise. Convolution with MHF showed the best detection rate. Even though MHF was described as a length-scale sensitive kernel (Buck et al., 2003), it generates nearly perfect results. The signal of the spherical marker is always similar to a Gaussian function; even the marker sizes are varied. Therefore, each marker with the same structure always produces higher responses than other components.

There are numerous limitations of this program. First of all, not all of the markers can be measured correctly; this suggests that the user interface should be implemented to enable user-interactive corrections. Secondly, marker identification is still a complicated procedure due to the fact that markers might be blocked or cannot be matched between pair images; therefore, a strong numbering algorithm that has the ability to deal with blocked or unmatched markers, is required. Thirdly, the accuracy of AFI-RSA is lower than UmRSA; this might be caused by the method of choosing a fitting model, so the

automated algorithm for selecting a fitting model should be improved. Last but not least, AFI-RSA was only evaluated in its ability to determine implant micromotion. Its performance in assessing another main field, polyethylene wear study in RSA, has not been conducted. While this novel program does have these limitations, it is more user-friendly and has accuracy and precision equivalent to that of the commercial software on the market. This novel program allows us to employ the RSA technique in a more efficient way.

The improved program was used for RSA projects in our lab, in order to improve the efficiency of the study, especially for those parts where the novel cage was utilized. The new program also has the potential to promote RSA studies in orthopaedic research, due to the fact that no specific knowledge is needed for the analysis of RSA radiography using this program.

3.5 References

Börlin, N., Thien, T., Kärrholm, J., 2002. The precision of radiostereometric measurements. Manual vs. digital measurements. J Biomech 35(1), 69-79.

Bragdon, C. R., Estok, D. M., Malchau, H., Karrholm, J., Yuan, X., Bourne, R., Veldhoven, J., Harris, W. H., 2004. Comparison of two digital radiostereometric analysis methods in the determination of femoral head penetration in a total hip replacement phantom. J Orthop Res 22(3), 659-64.

Buck, D., Alber, M., Nusslin, F., 2003. Potential and limitations of the automatic detection of fiducial markers using an amorphous silicon flat-panel imager. Phys Med Biol 48(6), 763-74.

Duvauchelle, P., Freud, N., Kaftandjian, V., Babot, D., 2000. A computer code to simulate X-ray imaging techniques. Nuclear Instruments and Methods in Physics Research Section B: Beam Interactions with Materials and Atoms 170(1-2), 245-258.

Gravel, P., Beaudoin, G., De Guise, J. A., 2004. A method for modeling noise in medical images. IEEE Trans Med Imaging 23(10), 1221-32.

Kärrholm, J., 1989. Roentgen stereophotogrammetry. Review of orthopedic applications. Acta Orthop Scand 60(4), 491-503.

Kärrholm, J., Herberts, P., Hultmark, P., Malchau, H., Nivbrant, B., Thanner, J., 1997. Radiostereometry of hip prostheses. Review of methodology and clinical results. Clin Orthop Relat Res(344), 94-110.

Madanat, R., Makinen, T. J., Moritz, N., Mattila, K. T., Aro, H. T., 2005. Accuracy and precision of radiostereometric analysis in the measurement of three-dimensional micromotion in a fracture model of the distal radius. J Orthop Res 23(2), 481-8.

Mäkinen, T. J., Mattila, K. T., Määttänen, H., Aro, H. T., 2005. Comparison of digital and conventional radiostereometric image analysis in an ankle phantom model. Scand J Surg 94(3), 233-8.

McCalden, R. W., Naudie, D. D., Yuan, X., Bourne, R. B., 2005. Radiographic methods for the assessment of polyethylene wear after total hip arthroplasty. J Bone Joint Surg Am 87(10), 2323-34.

Olsson, A., 2001. Automatic Roentgen Stereophotogrammetric Analysis. Centre for Mathematical Sciences. Lund University.Lund, Sweden, Master thesis.

Önsten, I., Berzins, A., Shott, S., Sumner, D. R., 2001. Accuracy and precision of radiostereometric analysis in the measurement of THR femoral component translations: human and canine in vitro models. J Orthop Res 19(6), 1162-7.

Ostgaard, S. E., Gottlieb, L., Toksvig-Larsen, S., Lebech, A., Talbot, A., Lund, B., 1997. Roentgen stereophotogrammetric analysis using computer-based image-analysis. J Biomech 30(9), 993-5.

Thistlethwaite, P. A., 2002. Computational methods in RSA: Application to acetabular components of total hip replacements. Mechanical Engineering. University of Calgary, Master thesis.

Vrooman, H. A., Valstar, E. R., Brand, G. J., Admiraal, D. R., Rozing, P. M., Reiber, J. H., 1998. Fast and accurate automated measurements in digitized stereophotogrammetric radiographs. J Biomech 31(5), 491-8.

Yuan, X., 2000. Accuracy analysis of RSA and development of RSPA. Department of Orthopaedics. University of Lund, Ph. D. thesis.

Yuan, X., Ryd, L., 2000. Accuracy analysis for RSA: a computer simulation study on 3D marker reconstruction. J Biomech 33(4), 493-8.

Yuan, X., Ryd, L., Blankevoort, L., 1997. Error propagation for relative motion determined from marker positions. J Biomech 30(9), 989-92.

4 Summary and Future Work

4.1 Summary

Radiostereometric Analysis (RSA) has been validated as the most accurate 3-D measurement tool in orthopaedic studies (Kärrholm, 1989; Kärrholm et al., 1997; McCalden et al., 2005). Its main applications focus on the evaluation of TJR performance. Even though RSA has a strong performance, assessment of novel surgical techniques and materials approximate its limitations, and require improvement in the accuracy and precision of RSA. At the same time, the many applications of RSA are limited by the complexity of 2-D measurement of RSA radiographs.

The objective of this project was to improve the function of RSA. In this thesis, we developed an enhanced calibration system to improve the accuracy and precision of RSA, and implemented an automated program to increase the user-friendliness of 2-D measurement. In Chapter 2, we examined the relationship between the calibration system and the performance of RSA, using numerical simulation. An optimal design for calibration cages, including calibration configuration and setup, number of calibration beads and displacement of calibration beads was acquired using the same approach. Before the physical manufacture of this new cage, an image simulation was conducted to predict its performance. A phantom study was then carried out to compare the new cage with two widely used ones, the uniplanar and biplanar cages. The results showed that the novel system improves the accuracy and precision of RSA by about 40% and 70%, respectively, when compared with these two widely accepted cages.

In Chapter 3, we evaluated the algorithms available for the measurement component of RSA, and implemented and modified the most advantageous ones in the enhanced program. The new program is fully automatic and was compared with the two commonly utilized commercial programs, UmRSA Digital Measure® (Biomedical Innovations AB, Umeå, Sweden) and RSA-CMS® (MEDIS Medical Imaging Systems

VB, Leiden, the Netherlands). These three programs have similar measurement accuracy and equivalent precision. To evaluate their user-friendliness, the measurement success rate, defined as number of markers measured successfully without any user-interactions over the number of markers which exist, was compared between the two fully automated programs, RSA-CMS and AFI-RSA. The results demonstrate an improvement of about 50% when using AFI-RSA. Last but not least, the new program is able to support the automated measurement of radiographs taken with the innovative cage developed in this project. The success rate of automated measurement is 96.3%.

In summary, we have successfully improved the function of RSA by developing and implementing an enhanced calibration system to improve its accuracy and precision, along with a superior program to increase user-friendliness. These two developments will be employed in our lab to evaluate the novel TJR techniques and materials, for which an extremely high accuracy and precision of RSA is required. Due to improved performance, these developments also have the potential to promote RSA in orthopaedic studies.

4.2 Future work

Although the novel cage has shown outstanding performance in phantom studies, further validation should be made under clinical circumstances in which the effects introduced by the patient are present, before it is applied in clinical studies. The automated program should also be tested with patient images before its application in clinical studies.

The accuracy and precision of RSA are the most important factors which make RSA a success. Its dependency on a calibration system, a good experimental setup, and radiography measurements have been investigated in this project and other studies (Yuan, 2000; Börlin et al., 2002). However, other issues related to image quality, e.g. grid and detector response, are unknown and their relationships with the accuracy and precision of

RSA should be studied. The image simulation procedure presented in this thesis could be utilized for this purpose without any physical limitations.

For the measurement component of RSA radiographs, several parameters in the software may still need manual adjustment due to the variety of image sizes and backgrounds. The algorithms of marker detection, centroid refining, and identification should be improved to develop a strong software that is able to perform successful measurement under complicated clinical circumstances, without any user interactions.

4.3 References

Börlin, N., Thien, T., Kärrholm, J., 2002. The precision of radiostereometric measurements. Manual vs. digital measurements. J Biomech 35(1), 69-79.

Kärrholm, J., 1989. Roentgen stereophotogrammetry. Review of orthopedic applications. Acta Orthop Scand 60(4), 491-503.

Kärrholm, J., Herberts, P., Hultmark, P., Malchau, H., Nivbrant, B., Thanner, J., 1997. Radiostereometry of hip prostheses. Review of methodology and clinical results. Clin Orthop Relat Res(344), 94-110.

McCalden, R. W., Naudie, D. D., Yuan, X., Bourne, R. B., 2005. Radiographic methods for the assessment of polyethylene wear after total hip arthroplasty. J Bone Joint Surg Am 87(10), 2323-34.

Yuan, X., 2000. Accuracy analysis of RSA and development of RSPA. Department of Orthopaedics. University of Lund, Ph. D. thesis, 90.

Appendix - Copyright releases from Elsevier

3 October 2007 Ref: CT/smc/Oct.2007.hsb013

ELSEVIER

Dear Rongyi Cai,

THE RADIOLOGY OF ORTHOPAEDIC IMPLANTS, 2001, ISBN 9780323002226, Pages 116-116, Freiberg, 'Chapter 6, 2 Figures only

As per your letter dated 15 August 2007, we hereby grant you permission to reprint the aforementioned material at no charge **in your thesis** subject to the following conditions:

1. If any part of the material to be used (for example, figures) has appeared in our publication with credit or acknowledgement to another source, permission must also be sought from that source. If such permission is not obtained then that material may not be included in your publication/copies.

2. Suitable acknowledgment to the source must be made, either as a footnote or in a reference list at the end of your publication, as follows:

   "This article was published in Publication title, Vol number, Author(s), Title of article, Page Nos, Copyright Elsevier (or appropriate Society name) (Year)."

3. Your thesis may be submitted to your institution in either print or electronic form.

4. Reproduction of this material is confined to the purpose for which permission is hereby given.

5. This permission is granted for non-exclusive world **English** rights only. For other languages please reapply separately for each one required. Permission excludes use in an electronic form other than submission. Should you have a specific electronic project in mind please reapply for permission.

6. This includes permission for the Library and Archives of Canada to supply single copies, on demand, of the complete thesis. Should your thesis be published commercially, please reapply for permission.

Yours sincerely

Clare Truter

Rights Manager